# Transit Hunt for Young and Maturing Exoplanets (THYME) VIII: a Pleiades-age association harboring two transiting planetary systems from *Kepler*

Madyson G. Barber,[1] Andrew W. Mann,[1] Jonathan L. Bush,[1] Benjamin M. Tofflemire,[2, *] Adam L. Kraus,[2] Daniel Krolikowski,[2] Andrew Vanderburg,[3] Matthew J. Fields,[1] Elisabeth R. Newton,[4] Dylan A. Owens,[1] and Pa Chia Thao[1, †]

[1]*Department of Physics and Astronomy, The University of North Carolina at Chapel Hill, Chapel Hill, NC 27599, USA*

[2]*Department of Astronomy, The University of Texas at Austin, Austin, TX 78712, USA*

[3]*Department of Physics and Kavli Institute for Astrophysics and Space Research, Massachusetts Institute of Technology, Cambridge, MA 02139, USA*

[4]*Department of Physics and Astronomy, Dartmouth College, Hanover, NH 03755, USA*

## ABSTRACT

We describe a young association (MELANGE-2) in the *Kepler* field harboring two transiting planetary systems (KOI-3876.01 and Kepler-970b). We initially identified MELANGE-2 by searching for kinematic and spatial overdensities around stars with high levels of lithium (in this case, KOI-3876). To better determine the age and membership of MELANGE-2, we combine archival light curves, velocities, and astrometry, with new high-resolution spectra of stars nearest KOI-3876.01 spatially and kinematically. The resulting rotation sequence, lithium levels, and color-magnitude diagram of members are all consistent with the Pleiades, confirming the population is co-eval and providing an age estimate of $105\pm10$ Myr MELANGE-2 may be one edge of the recently identified Theia 316 stream, also estimated to be $\simeq 108$ Myr. For the two planet hosts, we revise their stellar and planetary parameters, taking into account the newly-determined age. We fit the 4.5 yr light curve from *Kepler* and find that KOI-3876.01 is a $2.0\pm0.1 R_\oplus$ planet that orbits its star every 19.58 days orbit, while Kepler-970 is a $2.8\pm0.2 R_\oplus$ planet on a 16.73 day orbit. KOI-3876 was previously flagged as an eclipsing binary, but we rule this out using radial velocities from APOGEE and statistically validate the signal as planetary in origin. Given its overlap with the *Kepler* field, we expect MELANGE-2 to be valuable for studies of spot evolution on timescales of years and both planets to be a piece of the growing work on transiting planets in young stellar associations.

*Keywords:* exoplanets, exoplanet evolution, young star clusters- moving clusters, planets and satellites: individual (KOI3876)

## 1. INTRODUCTION

Stellar clusters and associations serve as critical benchmarks for stellar and planetary astrophysics. Stars in such groups formed from the same interstellar cloud, and hence share a common (or similar) age, abundance pattern, and initial space velocity. The common set of properties makes it significantly easier to assign prop-

Corresponding author: Madyson G. Barber

madysonb@live.unc.edu

* 51 Pegasi b Fellow

† NSF Graduate Research Fellow
  Jack Kent Cooke Foundation Graduate Scholar

erties to the whole population, providing age estimates that are more precise and accurate than general-purpose techniques used outside clusters (e.g., Gyrochronology; Barnes 2007; van Saders et al. 2016) and work on stars where ages are especially challenging (e.g., M dwarfs; Kiman et al. 2021). Such coeval associations are therefore, ideal for how studying how stellar and planetary properties evolve with time (e.g., Newton et al. 2021; Bouma et al. 2019; Krumholz et al. 2019).

Associations within the *Kepler* field have been especially valuable for stellar and planetary astrophysics. The $\simeq 4.5$ yr baseline and precise photometry enable precise measurements of rotation periods, even at older ages (e.g., Angus et al. 2015; Aigrain et al. 2015), providing

some of the best constraints we have on the rotation evolution of stars past 1 Gyr (Meibom et al. 2011; Curtis et al. 2019). The four *Kepler* clusters (NGC 6866, NGC 6811, NGC 6819, and NGC 6791) have also provided a wealth of information about stellar mass-loss (Miglio et al. 2012), post-main-sequence stellar evolution (Corsaro et al. 2012), and the occurrence of planets inside clusters (Meibom et al. 2013).

The four original clusters in the *Kepler* field are all at distances of more than 1 kpc and ages $\gtrsim$500 Myr (Batalha et al. 2010). While these older ages (compared to nearby young groups) fill an important niche in stellar spin down and post-main-sequence evolution, their distance from the Sun makes it challenging to study the low-mass members and search for small planets. The $K2$ mission covered many younger and more nearby clusters (Van Cleve et al. 2016; Rizzuto et al. 2017), but only for $\simeq$80 days at a time. Searching for long-period planets and studying longer-term spot evolution with $K2$ data was therefore only possible in regions that $K2$ covered by multiple campaigns (Rampalli et al. 2021). Any additional young associations in the *Kepler* field would provide the valuable $\simeq$4.5 yr baseline.

The availability of precise parallaxes and proper motions for millions of stars from *G*aia (Gaia Collaboration et al. 2016, 2021) has enabled the discovery of new coeval stellar associations (e.g., Meingast et al. 2019; Kerr et al. 2021), including the 40 Myr $\delta$ Lyr cluster that overlaps with the *Kepler* field (Bouma et al. 2021). The `FriendFinder` code[1] (Tofflemire et al. 2021) was designed to take advantage of *G*aia data, by searching for potential co-moving 'friends' around a user-identified young stars. This method has already been useful in finding the 250 Myr MELANGE-1 association (Tofflemire et al. 2021) and age-dating a planet in the Musca region of Lower-Centarus-Crux (Mann et al. 2021).

With the goal of finding undiscovered and confirming known associations with transiting planets, we ran `FriendFinder` on *Kepler* objects of interest with lithium levels indicating an age younger than Hyades Berger et al. (2018). The most promising association was a group of stars nearby KOI-3876; the candidate members showed a color-magnitude diagram (CMD) consistent with the Pleiades (consistent with the lithium levels). Here we describe our work demonstrating that the population (MELANGE-2) is a co-eval 105 Myr group, $\simeq$300 pc from the Sun, and harbors two transiting planetary systems (KOI-3876 b and Kepler-970 b).

[1] https://github.com/adamkraus/Comove

The *TESS* Hunt for Young and Maturing Exoplanets (THYME; Newton et al. 2019) was meant to focus on young planets identified with *TESS*, and the Zodiacal Exoplanets in Time (ZEIT; Mann et al. 2016a) survey aimed at those from $K2$. However, KOI-3876 b was flagged as young by the same team and using the same methods as used extensively in the THYME and ZEIT series. Since the planet is not along the ecliptic (Zodiac), we opted to include it in the THYME survey series with a slight adjustment to the acronym.

The paper is organized as follows. In Section 2 we detail our initial selection of potential members of MELANGE-2. We list the range of archival and new data taken on candidate members of MELANGE-2 in Section 3. In Section 4 we demonstrate MELANGE-2 is a co-eval population and derive its overall properties and basic membership. Our effort to find known and new planets in MELANGE-2 is described in Section 5. This includes the identification of another member with a confirmed planet (Kepler-970). We derive properties of the two identified planets in the association, KOI-3876 b and Kepler-970 b, in Section 7. The latter planet is already confirmed, and we statistically validate the former as planetary in Section 7.1. We summarize our findings in Section 8 and briefly discuss the future utility of an association overlapping the *Kepler* field.

## 2. TARGET SELECTION

As part of our effort to identify known planets in previously undiscovered young associations we ran the `FriendFinder` code (Tofflemire et al. 2021) on all stars identified as young based on their lithium absorption (Berger et al. 2018); this initial seed list included KOI-3876. The `FriendFinder` algorithm uses *G*aia EDR3 positions, parallaxes, and proper motions to identify stars with similar Galactic tangential velocity and $XYZ$ position to a selected input source. This required an absolute velocity for KOI-3876, for which we used the value from APOGEE (-26.79 km s$^{-1}$, Jönsson et al. 2020).

The lithium levels suggested an age for KOI-3876 close to the Pleiades (Bouvier et al. 2018). Unbound or weakly bound associations >100 Myr should be significantly dispersed as they orbit through the Galaxy (Krumholz et al. 2019). So we used a generous selection, including any star with a parallax uncertainty < 0.5 mas, a tangential velocity < 5 km s$^{-1}$ from KOI-3876 and a physical separation <50 pc from KOI-3876. This yielded 1007 candidates.

This selection assumed the group was circular and centered around KOI-3876, neither of which are likely to be true. However, our aim was not to make a perfectly clean list or a complete list of members. Rather, we aim

to select a generous list that contains enough members to derive an age for the planet hosts.

We show the color-magnitude diagram (CMD) for our candidate members in Figure 1. The spread of the CMD suggests significant contamination; it is likely that many of the 1007 stars selected are not associated with KOI-3876 (see Section 4.5 for more details). However, the CMD also shows a sequence of the closest stars (in tangential velocity) consistent with the Pleiades single-star sequence. This matches the age suggested by the Li levels in KOI-3876.
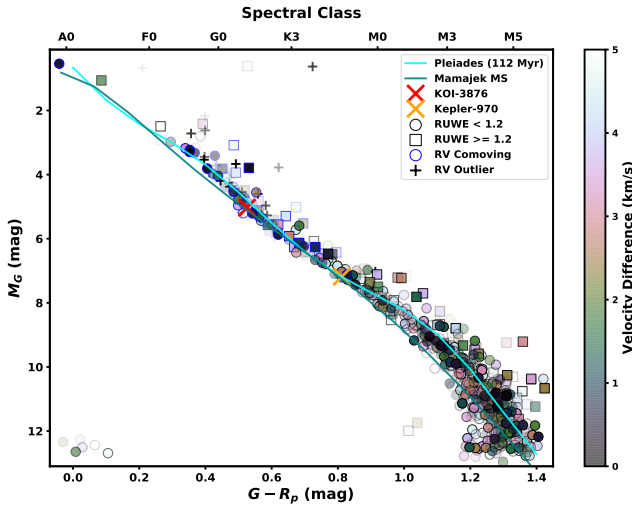


**Figure 1.** *G*aia color-magnitude diagram of all stars within $5\,\mathrm{km\,s^{-1}}$ in tangential velocity $50\,\mathrm{pc}$ (right) of KOI-3876. Approximate spectral types are shown on the top axis. Stars with a large `phot_bp_rp_excess_factor` for their color (Riello et al. 2021) are excluded. Points are color-coded by the difference between their expected and observed tangential velocity assuming a perfect $UVW$ match to KOI-3876 and transparency based on their distance from KOI-3876. Points with radial velocities consistent with KOI-3876 are marked with blue circles and those with discrepant velocities are changed to a plus signs (and excluded from the color coding). Approximate main Pleiades single-star sequences are shown as colored lines. These sequences are not corrected for reddening, and are only used as a rough guide.

## 3. OBSERVATIONS

### 3.1. *Optical spectra from McDonald 2.7 m Coudé*

We observed KOI-3876 and 21 association candidates (Section 2) with the Coudé spectrograph on the Harlan J. Smith 2.7m telescope at the McDonald Observatory. The Robert G. Tull Coudé is a cross-dispersed echelle spectrograph, delivering a R∼60,000 spectral resolution from 3400–10000 Å using the 1″.2 slit (Tull et al. 1995). Observations were taken over three nights from two ob-

serving runs, on 2021 July 9 and 2021 August 26 and 27. The sample was selected to include association candidates that could be observed with the Coudé in modest exposure times ($G < 13$), and spectral types later than mid-F ($B_p - R_P > 0.55$), where we expect lithium absorption to be a sensitive age diagnostic. The spectra are reduced with a custom python implementation of the standard IRAF procedures. Wavelength calibration made use of ThAr lamp spectra taken at the beginning, middle, and end of each night. The signal-to-noise of our spectra ranged between 14 and 60 per resolution element.

To assess whether association candidates are co-moving in three dimensions, we measure radial velocities using spectral-line broadening functions (BFs). The BF is a linear inversion of an observed spectrum with a narrow-lined template, and represents the average stellar absorption-line profile. This profile (the BF) can be fit with a rotationally-broadened line profile to measure the stellar radial velocity and $v \sin i_*$. We compute BFs for 34 spectral orders between 4300 and 9800 Åthat are free of telluric contamination using the `saphires` python package (Tofflemire et al. 2019). BFs from individual orders are combined in to a single, high SNR BF and fit with a rotationally broadened profile (Gray 1992). Narrow-lined templates, specific to each star, are taken from the Husser et al. (2013) PHOENIX model suite at the $T_{\mathrm{eff}}$ closest to that provided by the *TESS* Input Catalog (v8.0; Stassun et al. 2019). Radial-velocity errors depend on the S/N and rotational broadening, but are generally on the order of $0.1\,\mathrm{km\,s^{-1}}$. Measurements from the Coudé spectra are provided in Table 5.

### 3.2. *Kepler and TESS light curves*

#### 3.2.1. *Light curves for transit search and characterization*

We searched for *Kepler* photometry for all 1007 candidates within the Mikulski Archive for Space Telescopes (MAST). A total of 84 targets had *Kepler* data, the majority of which had data from all quarters (Q0-Q17). We restricted our analysis to long-cadence data (30 m), as short-cadence was not available for any of the candidate planet hosts and short cadence data is not needed for our transit search or rotation estimates. We also downloaded *TESS* photometry wherever it was available through MAST. This included 15 targets with 2-minute cadence data, and 41 targets with 30-minute cadence data from the Quick-Look Pipeline (QLP; Huang et al. 2020).

Where possible, we used the Pre-search Data Conditioning Simple Aperture Photometry (PDCSAP; Smith et al. 2012; Stumpe et al. 2012). This included KOI-3876, all *Kepler* candidate members, and the 15 targets

with 2-minute cadence from *TESS*. For the remaining, we used the Quick-Look Pipeline light curves (Huang et al. 2020) for our planet search. Table 5 lists which stars have *Kepler* and/or *TESS* photometry that was used for our planet search. More details on our transit search can be found in Section 5.

The remaining 885 sources had no pre-extracted *TESS* or *Kepler* light curves. We did not extract additional curves from the full-frame *TESS* images for our planet search or characterization. The association is more than 300 pc away; most of the remaining stars were too faint to extract a light curve precise enough for our planet search. However, many such systems are still useful for measuring rotation periods.

### 3.2.2. *Light curves and literature search for rotation*

To assess membership and age of MELANGE-2 members, we collect stellar rotation periods using literature measurements supplemented by our own measurements from *Kepler* and *TESS* light curves. First, candidate members were cross matched against Nielsen et al. (2013), McQuillan et al. (2013, 2014), and Santos et al. (2019, 2021) for literature rotation periods. We matched candidate members to catalog members by *Kepler* Input Catalog (KIC) identifiers, which are listed in each catalog. We identified 56 candidate members with available literature rotations, all but five of which have rotation measurements in multiple catalogs. For candidates that appear in only one catalog, we adopt the single measurement value. In cases where a star had measurements from more than one source, we adopt the average of the measurements as the rotation period. Only one object, KIC 3743810, had a conflicting rotation periods between catalog sources. Based on a visual examination of this object's *Kepler* PDCSAP light curve we selected the value from Nielsen et al. (2013).

For stars without literature rotation periods we performed our own analysis. Priority was given to *Kepler* PDCSAP data followed by *TESS* full-frame images. To generate the *TESS* light curves for rotation analysis, we first created raw flux light curves from the FFI cutouts centered on each candidate. Then, we generated a Causal Pixel Model (CPM) of the telescope systematics using the `unpopular` package (Hattori et al. 2021) for each individual star. We subtracted the CPM systematics from the initial light curves, resulting in the light curves used for our rotation search described in Section 4.2.

### 3.3. *Archival photometry and astrometry*

We download positions, parallaxes, proper motions, and $B_P$, $R_P$ and $G$ photometry for all candidate members of MELANGE-2 using the third *Gaia* Early Data Release (EDR3; Gaia Collaboration et al. 2021). For KOI-3876 and Kepler-970 (see Section 5), we also retrieved photometry from the Two-Micron All-Sky Survey (2MASS; Skrutskie et al. 2006), the Wide-field Infrared Survey Explorer (WISE; Cutri & et al. 2014), and the AAVSO All-Sky Photometric Survey (APASS; Henden et al. 2016). Photometry for KOI-3876 and Kepler-970 are listed in Table 3.

### 3.4. *Archival Velocities*

In order of preference, we drew radial velocities for candidate MELANGE-2 members from the second *Gaia* data release (DR2; Katz et al. 2019), the sixteenth APOGEE data release (DR16; Jönsson et al. 2020), and the fifth LAMOST data release (DR5; Luo et al. 2015, 2019). Velocities from our own spectra (Section 3.1) were given the highest priority. In the instance where a star had multiple velocities from the same star we used the weighted mean and error. We did not combine multiple velocities from different sources due to possible differences in the zero-points.

In total, we adopted *Gaia* RVs for 56 stars, APOGEE RVs for 5 stars, and LAMOST RVs for 25 stars. This was in addition to velocities from our Coude spectra for 22 candidate member stars as well as KOI-3876. We applied an offset to the LAMOST velocities of $+4.54$km s$^{-1}$ based on the comparison from Anguiano et al. (2018). There may be additional zero-point differences between the velocity sources, but these are likely larger than the internal velocity spread within the group. The adopted velocities are given in Table 5.

## 4. THE MELANGE-2 ASSOCIATION

As we show in Figure 2, radial velocities of candidate members are heavily clustered near the values we expect if their Galactic $UVW$ velocities match KOI-3876 within $\simeq 2$ km s$^{-1}$. The over-density is also highest for stars closer to KOI-3876 in tangential velocity and position.

Since the initial selection of targets was done without radial velocity information (Section 2) the abundance of similar radial velocities cannot be due to chance. Given the radial velocity of a expected typical thin disk star with similar $XYZ$ to KOI-3876 (Bochanski et al. 2007; Li et al. 2018), the probability of such a buildup by chance is negligibly small. We denote this group as MELANGE-2 (Membership and Evolution by Leveraging Adjacent Neighbors in a Genuine Ensemble), following the naming convention in (Tofflemire et al. 2021). As we discuss further in Section 4.6, it is likely part of the larger Theia 316 string (Kounkel & Covey 2019).

The distribution in Figure 2 also highlights the challenge; there is a significant population of stars with velocities far outside expectations for membership. Such
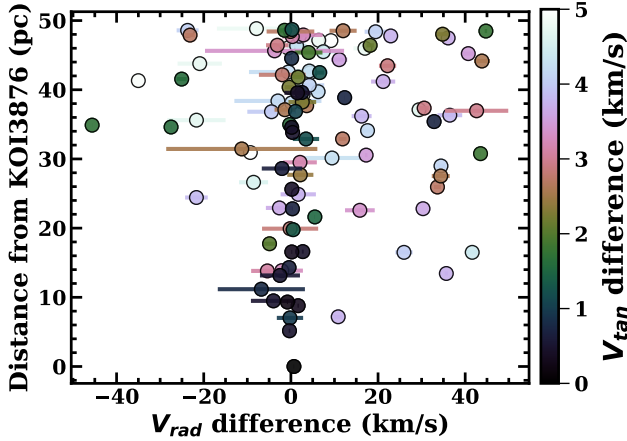
**Figure 2.** Distance from KOI-3876 as a function of the difference between the observed and predicted radial velocity of candidate members of MELANGE-2. The predicted velocities were calculated assuming each candidate has an identical $UVW$ to KOI-3876. KOI-3876 is not necessarily at the kinematic center of the group, the group has some intrinsic velocity spread, and many stars may be tight binaries; thus, we do not expect all true members to be exactly consistent with zero velocity difference. The over-density of points near zero velocity difference, particularly for those with similar tangential velocities to KOI-3876, confirms the association is real and likely extends to at least to 50 pc from KOI-3876.

contaminants include stars near KOI-3876 and Kepler-970 in position and tangential velocity. Further, the overdensity in velocity space is not necessarily co-eval; overdensities in kinematic space can occur for other reasons, such as dynamical perturbations from the Galactic bar (Bovy & Hogg 2010).

Our goal for the rest of this section is to demonstrate that MELANGE-2 is a single-age population and determine its age and basic kinematic and position properties.

### 4.1. *Lithium*

We measured the equivalent width of the Li 6708 Å line for 22 stars (including KOI-3876) using the Coude spectra described in Section 3.1. Using our measured radial and rotation velocities from the BF analysis, we shifted each spectrum to zero velocity and compared it to a rotationally broadened template of the same $T_{\rm eff}$. We then interactively defined regions of continuum between 6685 and 6730 Å, and the bounds of the EW integration. We measured the Li EW and its uncertainty using a bootstrap approach. The continuum was first fit using `emcee`, 1000 random draws from the fit posterior are used to normalized the spectrum, and for each realization, the Li absorption line is numerically integration 10 times where the integration bounds are varied randomly from a normal distribution with the width of a

resolution element. This procedure results in 10,000 Li EW measurements, we take the median and standard deviation as our final measurement and its uncertainty, respectively.

Past detections of Li with the same observational setup and our typical spectrum SNR indicate we were sensitive to Li down to equivalent widths of 20 mÅ or better. So we report this as our upper limit when no line is detected. One star (Gaia EDR3 2052858307226740352) had a $v \sin i_* > 50$ km s$^{-1}$, which made extraction of the Li line unreliable. So we instead reported a $< 70$ mÅ upper limit for this source based on earlier detections on similarly broadened spectra.

For KOI-3876, we estimated a Li equivalent width if 134 mÅ. This is marginally higher than (but consistent with) the value from Berger et al. (2018) (120 mÅ). We attribute this difference to Berger et al. (2018)'s removal of the Fe line at 6707.44 Å. We did not attempt to correct for this contamination or from broad molecular contamination in the cooler stars. Fe line contamination likely set a limit on the precision of our equivalent widths at the $\simeq 10\%$ level, comparable to the measurement errors. The difference was small compared to the offset in Li levels between clusters. We used our Li measurements for all targets for consistency.

Two spectra (Gaia EDR3 2101333021814076800 and 2048317736525727488) had two clear sets of lines, indicating SB2s. For our Li measurements, we measured each line individually with a manually-applied velocity offset. We then combined the two equivalent widths.

We compared the Li sequence for MELANGE-2 to that from the $\simeq 112$ Myr Pleiades Bouvier et al. (2018) and the 650-700 Myr Hyades from (Cummings et al. 2017) in Figure 3. The MELANGE-2 sequence is nearly identical to that from Pleiades. The Li sequences of nearby clusters from `BAFFLES` (Stanford-Moore et al. 2020) suggested an age between 85 Myr and 200 Myr This age range is conservative, as the bounds can only be set using the set of clusters with ages and extant lithium sequence measurements. For the upper bound, this was set by M34 and M35 (200-300 Myr).

### 4.2. *Rotation*

To better constrain the age and membership of MELANGE-2 (and hence KOI-3876 and Kepler-970), we attempted to determine rotation periods for all candidate members using *Kepler* rotation measurements from the literature or our own measurements from *Kepler* data or *TESS* full-frame images (FFIs). The light curve extraction and literature search are described in Section 3.2.2.
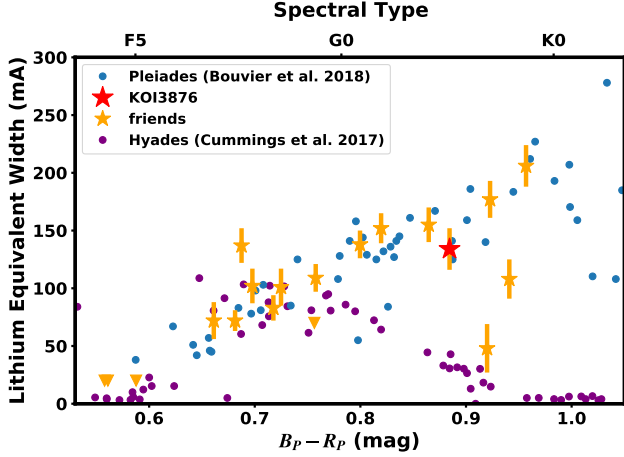
**Figure 3.** Lithium equivalent width as a function of $G$aia $B_P - R_P$ color for candidate members of KOI-3876 (MELANGE-2; orange), KOI-3876 (red), and members of the 125 Myr Pleiades from Bouvier et al. (2018) and $\simeq$700 Myr Hyades (Cummings et al. 2017). Triangles indicate upper limits. We have excluded MELANGE-2 candidates with velocities inconsistent with membership. The MELANGE-2 sequence is consistent with that from Pleiades members; only one star has an anomalously low Li (Gaia EDR3 2044150037698600448) compared to the Pleiades sequence. The high levels of Lithium seen in the mid-G dwarfs alone demonstrate that MELANGE-2 is much younger than Hyades.

For our own measurements, we searched the single-quarter *Kepler* or *TESS* light curves for rotation periods between $0.1 - 50$ days using the Lomb-Scargle algorithm (Horne & Baliunas 1986) for each quarter for each star with available *Kepler* data. We selected the initial rotation from the quarter returning the rotation period with the highest periodogram power. To confirm these measurements, we phase-folded the single-quarter light curves to the discovered period and examined the signals' consistency across quarters. We performed an eye-check in the style of Rampalli et al. (2021), labeling obvious rotations as Q0, questionable rotations as Q1, spurious detections as Q2, and non-detections as Q3. In total, 11 of the stars with *Kepler* data and no literature rotation returned usable rotations of quality Q0 or Q1.

For the rest of the candidates without rotations found in the literature or through our *Kepler* light curve measurements, we searched for signatures of rotation in CPM light curves extracted from the *TESS* Full Frame Image data (see Section 3.2). After searching each single-sector light curve of each star for rotation periods from $0.1-30$ days using the Lomb-Scargle algorithm, we repeated the same rotation selection and quality check procedure as outlined for the *Kepler* data. We found

64 quality Q0 or Q1 rotations from the *TESS* CPM-subtracted light curves available.

Based on variations in the extracted rotation period between *TESS* sectors and/or *Kepler* quarters, we estimate rotation period errors to be $\simeq$10% for our own measurements. This larger than the expected errors just considering signal-to-noise and Lomb-Scargle errors from bootstrapping, likely due to differential rotation and spots appearing and disappearing on the surface of the star.

In total, we were able to assign rotation periods to 131 candidate members, all of which are reported in Table 5; 67 periods were determined based on *Kepler* data and 64 from *TESS*. The rotation period distribution (Figure 4) is consistent with that from the Pleiades, further validating the age from our Li measurements. Approximately 92 of these have rotation periods consistent with the Pleiades sequence. Most of the slower rotators are likely field interlopers, as they are (statistically) further from KOI-3876 in both three-dimensional distance and tangential velocity.

Of 1007 initial candidates, only having 92 stars with Pleiades-like rotation periods initially appears as a low success rate for a young association. However, for the overwhelming majority of the other 876 stars, no rotation period could be measured even if one is present (mostly due to intrinsic faintness). For example, of the 935 stars with a matching TIC ID, but no rotation period from *Kepler* data, 751 were either too faint ($T \gtrsim 15$) or too contaminated by nearby stars to extract a usable CPM curve. An unknown further set of stars had light curves but may have had rotation amplitudes below detectable levels due to poor SNR. Thus, the difference is mostly a measure of how $G$aia can retrieve precise astrometry for stars far fainter than *Kepler* and *TESS* can provide rotation periods for.

### 4.3. *Isochronal age*

We estimated the age of MELANGE-2 by comparing the CMD to the PARSEC (v1.2S) models (Bressan et al. 2012). We used a mixture model, as detailed in Mann et al. (2021)[2], based on the method outlined in Hogg et al. (2010), and wrapped in a Monte-Carlo Markov-Chain using `emcee` (Foreman-Mackey et al. 2013). To briefly summarize, we fit the population with the combination of two models. The first described the single-star member sequence drawn from PARSEC models. The second is an outlier population, which may itself contain a mix of populations (e.g., binaries, field interlopers, and
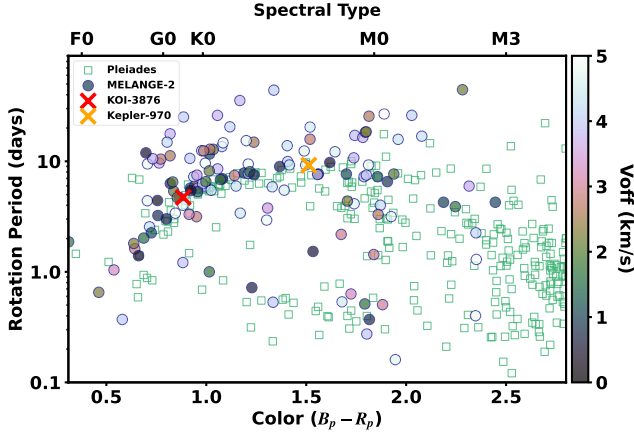
---

[2] https://github.com/awmann/mixtureages

**Figure 4.** Rotation periods candidate members of MELANGE-2 (dark circles). Only literature measurements or stars with Q0 or Q1 rotations are shown. For reference, we show rotation periods from $\simeq$110 Myr Pleiades (green squares; Rebull et al. 2016a). Stars are color-coded by their tangential velocity difference compared to KOI-3876. Statistically, the stars on the Pleiades gyrochrone are also closer to KOI-3876 in tangential velocity. Because of the distance to the cluster, we have few rotation periods past M1.

stars with erroneous parallaxes or photometry). The fit included six free parameters: the association age (age), the average reddening across the association ($E(B-V)$), the amplitude of the outlier population ($P_B$), the offset of the outlier population from the main population CMD ($Y_B$ [mags]), the variance of the outliers around the mean ($V_B$ [mags]), and a term to capture missing uncertainties or differential reddening across the association ($f$ [mags]).

Reddening was limited to $< 0.2$ mag based on the three-dimensional extinction map from Green et al. (2019). All other parameters evolved under uniform priors, bounded only by physical limits. To ensure uniform sampling in age, we re-sampled the model grid in equal steps around the expected age (50-300 Myr). Using the raw grid did not significantly change the results.

$G$aia photometry was available for all candidate members, and was generally far more precise than other available photometry. Many stars were also resolved as binaries (or the target and a background star) in $G$aia, but seen as a single source in 2MASS and KIC photometry (Brown et al. 2011). So we restricted our analysis to $G$aia magnitudes.

While the mixture model can handle high contamination rates by making $P_B$ larger, tests suggest that when $P_B \gtrsim 0.4$, the model often calls stars in the main population outliers, instead fitting the background population as the true one (yielding a field age). As we show in Section 4.5, the background contamination rate is compara-

ble. Further, for the purposes of the isochrone analysis, there will be additional true members that should be treated as as outliers due to binarity, poor photometry, or poor parallaxes. In addition to limiting the sources to objects within the colors and magnitudes bounded by the model grid, we limited the input list to stars satisfying the following criteria:

- a renormalised Unit Weight Error (RUWE; Gaia Collaboration et al. 2021) $< 1.3$,

- $1.0+0.015(B_P-R_P)^2 <$ `phot_bp_rp_excess_factor` $< 1.3 + 0.06*(B_P-R_P)^2$,

- physical separation within 40 pc of KOI-3876,

- tangential velocity within 4 km s$^{-1}$ of KOI-3876,

- a radial velocity within $3\sigma$ of the group or no radial velocity.

The final criterion included removing of the handful of white dwarfs seen in the CMD (Figure 1).

These cuts were designed to mitigate, but not not completely remove, issues of binarity, data quality, non-member interlopers, as well as limitations of the models. The mixture model approach means they do not need to completely remove bad data or non-members. Taken individually, none of these had a significant impact on the derived age except the `phot_bp_rp_excess_factor` criteria. Stars with flux contamination tended to have CMD positions far *below* the main-sequence. After all cuts we were left with 205 stars.

As we show in Figure 5, the resulting fit yielded an age of $106^{+7}_{-6}$ Myr. As a test of the systematic errors, we ran the same fit using models from the Dartmouth Stellar Evolution Program (DSEP, Dotter et al. 2008). Using the DSEP models with magnetic enhancement described in Feiden & Chaboyer (2012) gave a similar age of 101±7 Myr. DSEP models without magnetic enhancement gave a younger age of 96±10 Myr, although a poorer fit to the coolest stars in the sample. Using (PARSEC) non-Solar metallicity models with changed the age at the $\lesssim$ 5 Myr level, but favoring older ages. All ages agree with each other at the 1-2$\sigma$ level. These ages are also consistent with our measurements using lithium and stellar rotation (Sections 4.2 and 4.1), both of which indicated an age close to Pleiades ($\simeq$112 Myr; Dahm 2015). Based on all analyses we adopt an age of 105 ± 10 Myr.

### 4.4. Galactic Position and Kinematics

For each of the 1007 candidate members of MELANGE-2, we show show the Galactic $XYZ$ position in Figure 7 and the proper motion in Galactic
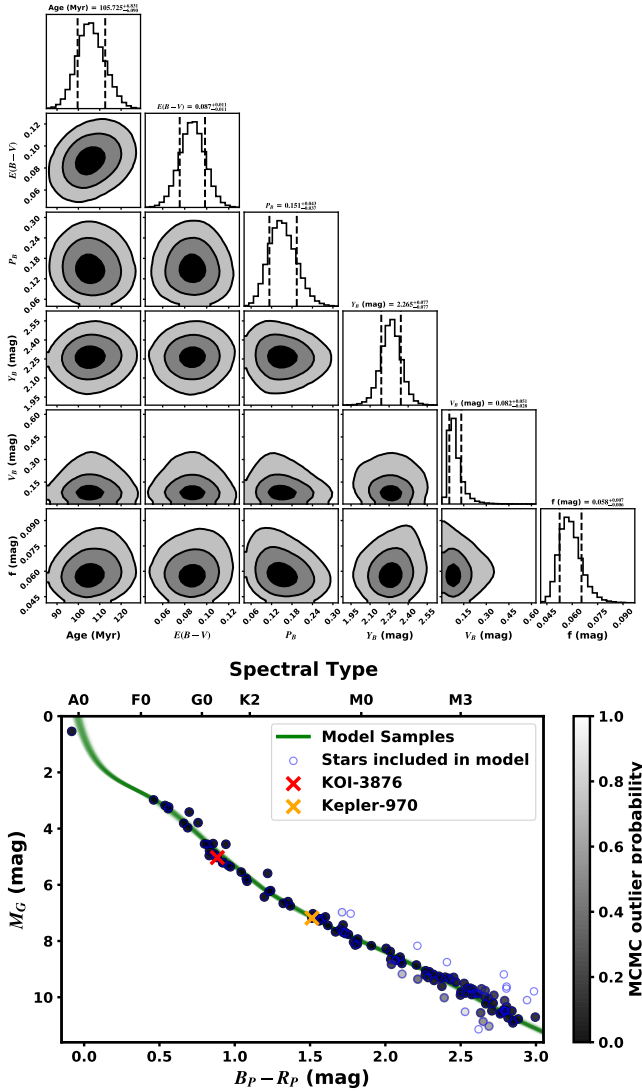
**Figure 5.** Comparison of the PARCSEC model isochrones to candidate members of MELANGE-2. The top shows the corner plot of our MCMC mixture model comparison, with contours corresponding to $1\sigma$, $2\sigma$, and $3\sigma$. The bottom plot shows the *G*aia $G$ versus $B_P - R_P$ CMD of stars included in the MCMC (blue circles). Each point is shaded based on their average outlier probability as determined by the relative strength of the two mixture components. Most of those flagged as outliers are likely to be non-members or binaries. KOI-3876 and Kepler-970 are shown as red and orange stars. Both have low ($< 1\%$) outlier probabilities. The green lines are 200 PARSEC isochrones with parameters drawn (randomly) from the MCMC posterior.

coordinates ($l$, $b$) in Figure 6. While there is a clear overdensity of sources within $\simeq 1$km s$^{-1}$ of KOI-3876, our initial selection included a large number of field interlopers. A tighter cut on velocity and distance would lower contamination, but some sources far in separation have matching velocities and show other signs of youth

**Table 1.** Properties of MELANGE-2

| Parameter | Mean | $\sigma$ |
|---|---|---|
| $X$ (pc) | 103 | 19 |
| $Y$ (pc) | 289 | 18 |
| $Z$ (pc) | 63 | 14 |
| $U$ (km s$^{-1}$) | -9.2 | 1.4 |
| $V$ (km s$^{-1}$) | -25.54 | 0.36 |
| $W$ (km s$^{-1}$) | 1.0 | 1.2 |

(such as rotation). This makes it challenging to derive the $UVWXYZ$ parameters of the association from the full membership list.

Instead, we select a set of high probability members independent of their *G*aia parameters that were used for initial selection. Unlike for fitting the isochrones, the low-mass stars offer no particular advantage. So we opted to included only sources with a rotation period consistent with the Pleiades sequence and those with radial velocities within 8km s$^{-1}$ of the source. We removed three additional targets that had low-precision velocities (from LAMOST).

The cuts left us with 31 high-probability members. From these we estimate the Galactic position ($XYZ$) and kinematic ($UVW$) parameters, as well as the clusters in each parameter ($\sigma_X$, $\sigma_Y$, $\sigma_Z$, $\sigma_U$, $\sigma_V$, and $\sigma_W$) after accounting for measurement errors. The resulting parameters are given in Table 1.

A more formal treatment would account for covariance between these parameters (e.g., Gagné et al. 2018). However, the group may actually be part of a much larger stellar string, which would require a different model (Kounkel & Covey 2019; Gagné et al. 2021). We discuss this possibility in more detail in Section 4.6. Since we were primarily interested in characterizing the planets, we defer a more detailed analysis of MELANGE-2 and its relation to other groups for a future analysis focused on the association.

### 4.5. *Contamination Rate*

Based on a qualitative inspection of the proper motion and $XYZ$ positions (see Figures 6 and 7), we expect many of our 1007 candidate members are field interlopers. We can make a more quantitative estimate of the contamination rate using our rotation and radial velocity measurements. These are particularly effective because neither metric was used in our initial sample selection (`FriendFinder` only used the velocity of KOI-3876).
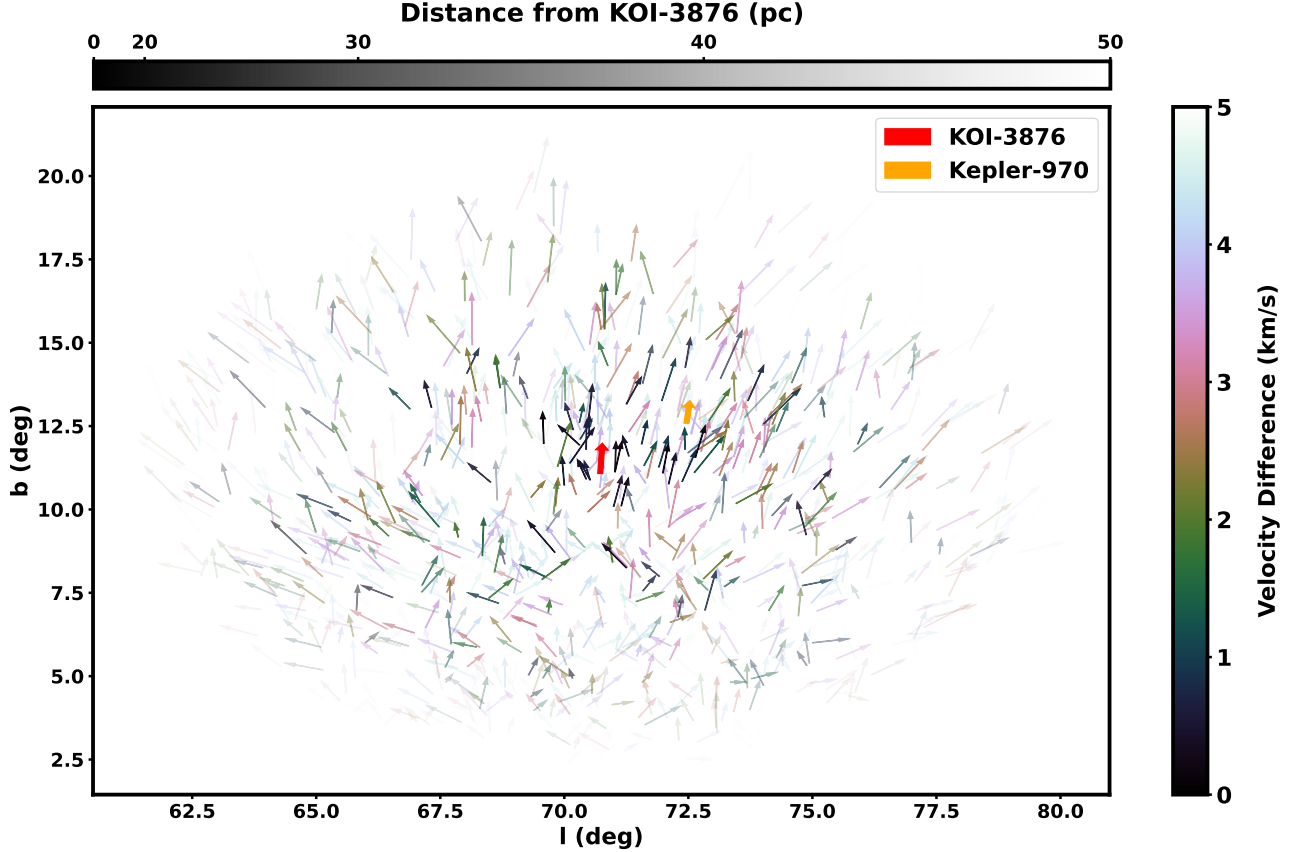
**Figure 6.** Galactic coordinates and motions for all 1007 candidate members of MELANGE-2. The red arrow shows KOI-3876, Kepler-970 is shown in orange, and other stars are color-coded by their tangential velocity offset from KOI-3876 with transparency set by their physical distance from KOI-3876. Arrows indicate the direction and (relative) magnitude of the proper motion.

We first estimated the contamination rate from the ratio of the number of stars with rotation periods consistent with the Pleiades sequence compared to the total number of stars *for which we could estimate a reliable rotation period.*

For the numerator (number of stars with rotation periods consistent with the Pleiades) we used a three-step cut. The first cut required stars with a $Bp - Rp < 0.7$ to have a rotation period $\leq 3$ days. The second cut required stars with $0.7 \leq Bp - Rp < 1.0$ to have a rotation period $\leq 7.5$ days. The third cut required stars with $Bp - Rp \geq 1.0$ to have a rotation period $\leq 10$ days. We note that these cuts are somewhat qualitative, but designed to capture $> 95\%$ of the Pleiades rotators (see Figure 4) and remove most field stars. These cuts yielded 92 stars consistent with the Pleiades rotation sequence.

The denominator is effectively the number of stars that would pass the above cut if every single star was a member. *Kepler* light curves were extracted to search

for planets (Jenkins et al. 2010), which is generally a much smaller signal than the rotation signal of $\simeq 100\,\mathrm{Myr}$ stars. Thus, we assumed we could extract a rotation period for any member with a *Kepler* light curve. For *TESS*, we used the recovery fraction from the *TESS-K2* overlap described in Bush et al. (in prep). The recovery rate is a strong function of magnitude, with almost no periods recovered past $T_{\mathrm{mag}} = 15$ and a 63% recovery rate for $14 < T_{\mathrm{mag}} < 15$ that increases down to the brightness limit. Based on this, we expect to measure 82 rotation periods in the *TESS* data.

Of these 156 stars, 92 have rotation periods consistent with Pleiades. This suggests about 59% of candidate members are true members. This estimate does not account for stars where the rotation periods are consistent with $\lesssim 100\,\mathrm{Myr}$ by chance. Roughly, assuming field stars are uniformly distributed from 0–10 Gyr, the number of candidates matching by chance should be $\lesssim 1$. A more significant problem would be tight binaries, where the inferred rotation periods would be fast due to tidal lock-
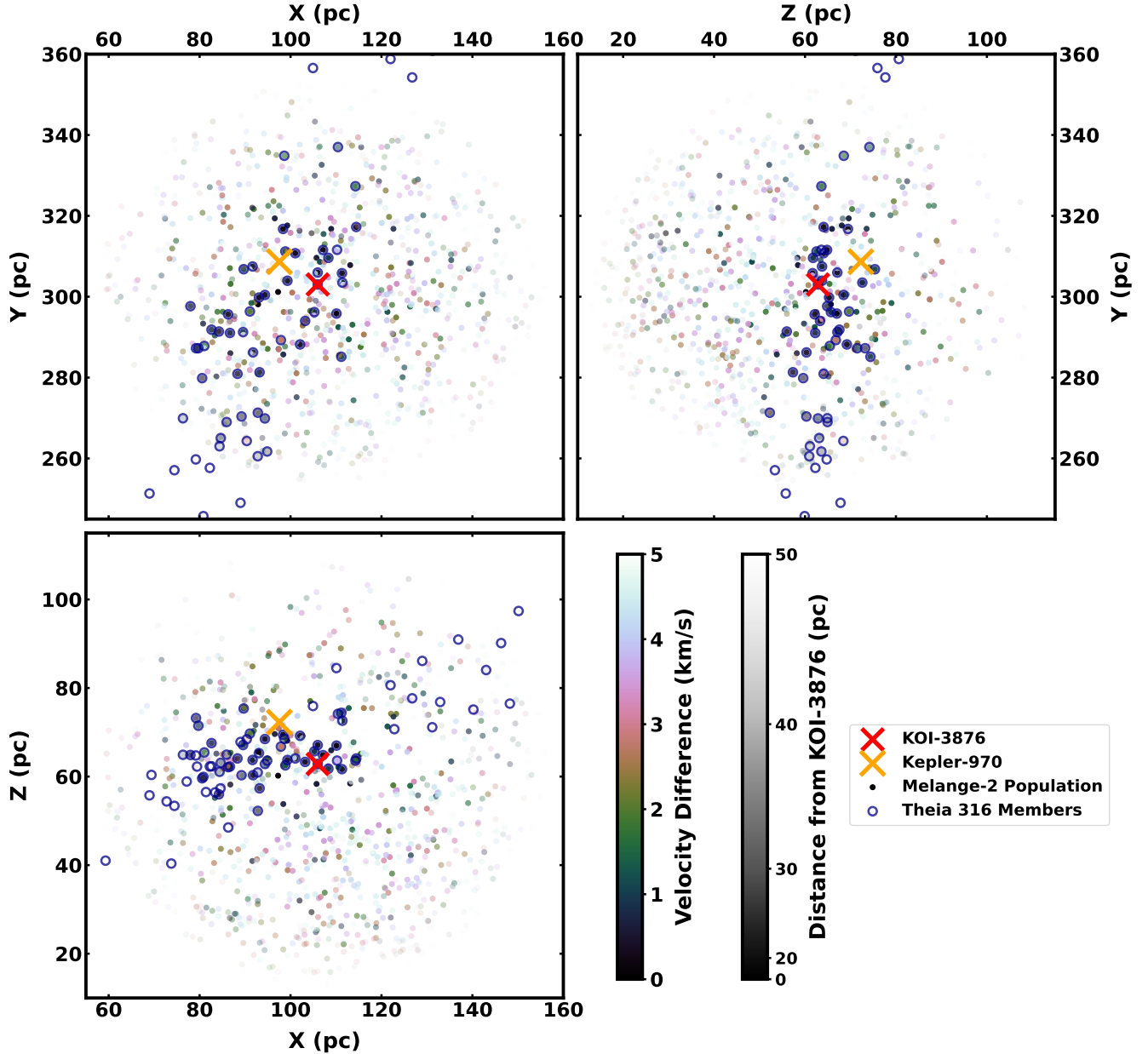
**Figure 7.** Galactic Heliocentric (XYZ) coordinates of stars within 50pc and 5km/s of KOI-3876, color-coded by their velocity difference from KOI-3876and transparency set by their distance from KOI-3876. KOI-3876 is shown as a red X, Kepler-970 as an orange X, and members of Theia 316 from Kounkel & Covey (2019) as blue hollow circles.

ing or the star spun down at a slower than normal rate due to the influence of the companion. We may also miss a small number of stars due to low spot modulation, although past rotation period surveys suggest this is < 10% (e.g., Rebull et al. 2016a; Douglas et al. 2017, 2019).

We performed a similar test using the radial velocities, effectively asking what fraction of the stars are consistent with the group velocity. Assuming an internal velocity dispersion of 0.5–1km s$^{-1}$ (Section 4.4), 52%–57%

of the candidate members with velocities are within $3\sigma$ of the expected radial velocity for membership.

Based on a random selection of stars from $G$aia in the same part of $XYZ$ space, a typical star in will have a velocity $\simeq 25$km s$^{-1}$ lower than MELANGE-2, but with a spread that overlaps. This can be seen in the asymmetric distribution of stars in Figure 13. Thus, as with rotation, we expect $\simeq 5\%$ of the selected stars to be consistent by chance. This is similar to or smaller than the number of real members that appear inconsistent with

the population because of underestimated uncertainties in the radial velocities and spectroscopic binaries.

The two estimates are broadly consistent with each other given the uncertainties and complicating factors. We conclude 50-60% of the 1007 candidate list are real members of MELANGE-2.

### 4.6. *Connection to Theia 316*

Kounkel & Covey (2019) identified a number of young stellar associations using from *G*aia DR2 data. One such string, Theia 316, includes KOI-3876. Kounkel & Covey (2019) estimate an age for Theia 316 of 108 Myr, consistent with our own estimate for MELANGE-2. This suggests that MELANGE-2 is a component of the larger Theia 316 string.

As we show in Figure 7, the populations show significant overlap in $XYZ$ space. Many stars in Theia 316 are missing from our list of MELANGE-2 candidates, the great majority of which are more than than 50 pc from KOI-3876 (our `FriendFinder` adopted search radius). This is because the density clustering method used in Kounkel & Covey (2019) had no restrictions on the physical size of the group, as long as the number of sources in a given spatial and proper motion space is sufficiently dense. By contrast, `FriendFinder` was designed to help age-date a specific star, and hence identifies targets within a given radius in kinematic and physical space. Increasing the search radius on `FriendFinder` would likely help us recover some of the missing stars, but also increase the contamination rate and thus unlikely to improve our ability to assign ages to the two planet hosts.

Similarly, many high-probability members of MELANGE-2 are missing from the Theia 316 list (including Kepler-970). There are 40 stars that match expectations for membership in MELANGE-2 in at least two of the following: rotation period, radial velocity, and lithium levels. Based on the distribution of the background population, we expect >85% of these 40 stars to be real members. However, only 15 of them are on the Theia 316 list. Using the (slightly different) high-probability member list in Section 4.4 or similar cuts yield almost identical conclusions; slightly more than half the real members are missing from the Theia 316 list.

### 5. SEARCH FOR PLANETS IN MELANGE-2

To check for other candidate planets or eclipsing binaries in the same association we searched *Kepler* and *TESS* light curves using the Notch pipeline[3] as de-

---

[3] https://github.com/arizzuto/Notch_and_LOCoR

scribed in Rizzuto et al. (2017). To briefly summarize, the Notch filter fits a window of the lightcurve as a combination of an outlier-robust second-order polynomial (for the stellar variability) and a trapezoidal notch (representing the potential planet). The window moves along the lightcurve until the variability is detrended while preserving the planet signal. At each data point, we calculate the improvement from adding the trapezoidal notch based on the change in the in Bayesian Information Criterion (BIC) compared to modelling just a polynomial. It then repeats this process over the full curve.

We searched the detrended light curves and the BIC signals that Notch produces for periodic signals. We excluded the rotation period (and aliases) of the star that arise from imperfect detrending. We also checked for known *Kepler* objects of interest (KOIs) within candidate members of MELANGE-2, identified by a simple cross-match against the most recent KOI catalog (Twicken et al. 2016). All but one of these were flagged by the Notch search.

In total, we identified 18 targets of interest that pass the SNR and initial quality checks from Notch. Eight of these are known KOIs (KOI-678.01, KOI-678.02, KOI-966.01, KOI-966.02, KOI-1838.01, KOI-5304.01, KOI-6819.01, and KOI-7059.01), while the remaining are newly identified. All 18 targets are listed in Table 2 along with our classification of each. Other than KOI-3876 b, we identified only one other system (Kepler-970 b) that was both likely to be a real planet and a member of MELANGE-2. We discuss each system and our reasons for rejection them below.

### 5.1. *Discussion of individual candidates*

KOI-678 (.01 and .02) contains two confirmed planets (Kepler-211 bc), and the star's light curve showed a clear rotation signature of $\simeq 13.7$ days. However, this period is too long for membership given its *G*aia colors (should be $\lesssim 8$ days). Similarly, the lithium equivalent width is only 3.8mÅ (Berger et al. 2018), but membership would suggest a Li level above 100mÅ. The star's proper motion also puts it on the outskirts of the distribution. We conclude this target is unlikely to be a member.

Both planet candidates in KOI-966 are flagged as false positives by the *Kepler* analysis (Coughlin et al. 2016), with both signals attributed to an eclipsing binary (.02 corresponding to an alias of the secondary eclipse). We similarly concluded that the signal is likely an eclipsing binary based on the V-shaped transit and secondary eclipse. The star's rotation period (3.92 days; Walkowicz & Basri 2013) is consistent with membership for an M dwarf and does not match the eclipse period

(0.379 days). The star is also only 1km s$^{-1}$ and 8 pc from KOI-3876, near the core of likely members. We conclude it is likely an eclipsing binary in the association.

KOI-1838.01 is a confirmed planet (Kepler-970 b; Morton et al. 2016). The star's rotation (9.23 days) places it right on the Pleiades sequence (see Figure 4), and much faster than the stalling regime seen for > 600 Myr systems (Curtis et al. 2019). The LAMOST (corrected) velocity is -32±4 km s$^{-1}$, which is consistent with the value predicted for membership ($\simeq$-27km s$^{-1}$). A more precise measurement from the CKS-cool project Petigura (in prep) yielded an RV of -27.15±0.10km s$^{-1}$, an excellent match for the association. The corresponding high-resolution spectrum from Petigura (in prep) shows weak lithium ($< 40$mÅ), but this is consistent with 100 Myr for its spectral type (Baraffe et al. 2015). As we show in Figures 1, 6, and 7, Kepler-970 lands on the expected CMD for a Pleiades-aged star and is nearby other likely members both in Galactic position and proper motion. We conclude that this planet is real and a member and include it in our analysis through the rest of the paper.

KOI-5304.01 was flagged as a false positive by the *Kepler* analysis due to a non-transit-like shape. Our visual inspection of the candidate agrees with this. The host star also shows a measurable but slow rotation period of $\simeq$11.4 days, which is slower than expected for membership (see Section 4.2). We conclude that this is a false positive and not a member.

KOI-6819 contains a planet candidate (.01). The star shows no significant rotation, suggesting the star is of older age. The *G*aia DR2 velocity for KOI-6819 is 3.27km s$^{-1}$, $\simeq$20km s$^{-1}$ from the expected for membership in the association. We conclude this target is unlikely to be a member.

KOI-7059.01 is flagged as a false positive by the *Kepler* analysis (Coughlin et al. 2016), and the odd-even depth difference strongly suggests and eclipsing binary. The APOGEE velocity is $\simeq$8km s$^{-1}$ from the cluster. The discrepant velocity may be due to binarity, but the source also lands on the outskirts of the membership list, >48 pc from KOI-3876 and near the edge in terms of tangential velocity. We conclude this target is likely a real eclipsing binary and unlikely to be a member.

The newly identified targets, KIC 6366739 and TICs 20352534, 237181417, 272486188, 28768382, 138966713, 158168145, 158415341, 164678171, and 355909811, were all initially flagged as potentially interesting signals. TIC 272486188, 164678171, and 158415341 have both *TESS* and *Kepler* data, but we could not recover the transit signals we identified from *TESS* data in the higher-quality *Kepler* data. Figure 8 shows TIC 158415341 as an example of this. We see a poten-
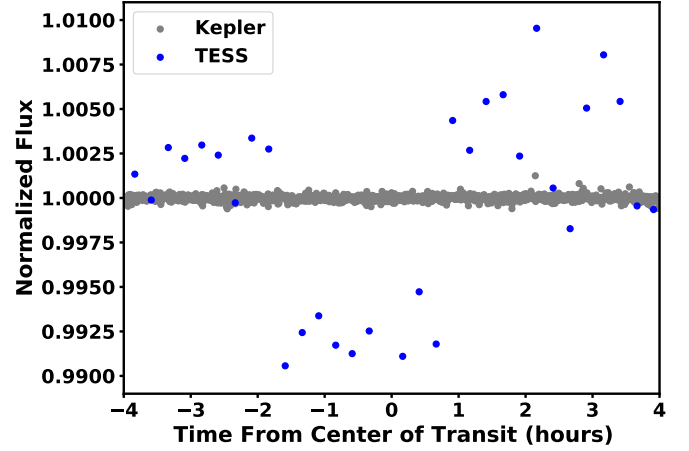


**Figure 8.** Phase-folded light curve of potential member TIC 158415341 from *TESS* (blue) and *Kepler* (grey) detrended with the Notch filter. We find TIC 158415341 has a best fit period of 20.016 days with an initial transit time of 1690.503 BTJD using *TESS* data, but we fail to detect the transit using *Kepler* data. We reject this signal as noise in the *TESS* data.

tially interesting transit in *TESS*, but we failed to recover TIC 158415341's (KIC 9700914) transit signal in the *Kepler* data. KIC 6366739 shows signs of a possible signal in the *Kepler* photometry. However, the candidate has a long period (22 days) and was observed for only a single quarter, so the SNR was insufficient. When using Notch, TICs 20352534, 237181417, 28768382, 138966713, 158168145, and 355909811 passed the BIC criterion for significance, but upon further visual inspections, we find the transit signals did not have the expected transit shape and are more easily explained as systematics or imperfectly removed stellar noise.

TICs 272486188, 158415341, and 164678171 are unlikely to be members of MELANGE-2 as the radial velocity measurements are >20km s$^{-1}$ from the predicted values for membership.

KIC 6366739 is unlikely to be a member since the rotation period is $16.9 \pm 1.3$ days, which is greater than expected for this association.

TICs 138966713 and 158168145 are likely members of the association. TIC 138966713 has a radial velocity of $-29.9 \pm 10.0$ km s$^{-1}$, consistent with the expected radial velocity. TIC 158168145 has a radial velocity $-24.4 \pm 1.1$ and a rotation period $5.4 \pm 0.5$, both of which are consistent with the expected values.

TICs 20352534, 237181417, and 355909811 do not have available rotation periods, radial velocities, or Lithium measurements, but we conclude all are unlikely to be members. While TIC 20352534 is likely young since it is an A-type, the star is on the edge of the search region (49.34 pc from KOI-3876) and the edge of the tan-

gential velocity difference allowance (4.45 km s$^{-1}$ from KOI-3876). It is possible TIC 20352534 is a member, but it is unlikely. TICs 237181417 and 355909811 show no signs of rotation, indicating they are most likely older stars not apart of the association.

## 6. PROPERTIES OF KOI-3876 AND Kepler-970

We summarize constraints on both host stars in Table 3, the details of which we provide below.

### 6.1. *Literature Parameters*

As a reasonably bright ($K_P = 12.6$) star hosting a planet candidate from the *Kepler* mission, KOI-3876 has numerous stellar parameters in the literature. The California *Kepler* Survey (CKS) estimate $T_{\rm eff}$=5720 ± 60 K, $log\ g$ =4.64±0.1, and $v \sin i_*$=9.9±1.0km s$^{-1}$, $R_*$0.95$^{+0.06}_{-0.04}R_\odot$ and $M_* = 1.01 \pm 0.03M_\odot$ based on comparing their high-resolution spectra and comparison to well-characterized templates (Petigura et al. 2017; Yee et al. 2017) and stellar isochrones (Johnson et al. 2017). Brewer & Fischer (2018), using the same spectra, estimate $T_{\rm eff}$=5642±27 K, $log\ g$ =4.46±0.05, $R_* = 0.93 \pm 0.02M_\odot$, $M_* = 0.99 \pm 0.02M_\odot$, and $v \sin i_*$=10.4±0.5km s$^{-1}$, as well as detailed abundances that are generally consistent with the Solar value. Berger et al. (2020) incorporated *G*aia DR2 data with MIST stellar isochrones to derive an $T_{\rm eff}$=5577 ± 85 K, $log\ g = 4.50 \pm 0.02$, and $R_* = 0.908 \pm 0.017R_\odot$.

For Kepler-970, Berger et al. (2020) estimated $T_{\rm eff}$=4314±73 K, $log\ g = 4.63 \pm 0.02$, $R_* = 0.649 \pm 0.012R_\odot$, and $M_* = 0.657 \pm 0.022M_\odot$ using the *G*aia parallax, photometry, and MIST isochrones as with KOI-3876. Based on the CKS spectra, Petigura (in prep) found a consistent $T_{\rm eff}$ (4401±70 K), stellar radius ($R_* = 0.70 \pm 0.03R_\odot$), and mass ($M_* = 0.68 \pm 0.10M_\odot$). Petigura (in prep) also estimated a $v \sin i_*$ of 5.21±1.0km s$^{-1}$ from the CKS spectra. This $v \sin i_*$ may be slightly overestimated due to mild broadening in their templates, but the errors are sufficiently generous for our analysis.

These stellar parameters are generally in agreement with each other. However, literature estimates that relied on model isochrones (e.g., Berger et al. 2020) assigned > 2 Gyr ages for both stars, much older than the true ≃100 Myr age from the association. Although the assigned age uncertainties were large, the derived parameters may still be biased by the lack of an assigned age. Although this will not impact purely spectroscopic parameters like $T_{\rm eff}$ and $v \sin i_*$, the assumption can have a strong impact on the estimated stellar mass. Thus, we revisit these parameters with our own analysis below.

### 6.2. *Spectral-Energy Distribution*

We fit the observed spectral-energy-distribution (SED) of both stars following Mann et al. (2016b). To briefly summarize, we fit the observed photometry with a grid of optical and near-infrared flux-calibrated spectra spanning 0.4–2.3$\mu$m. We included BT-SETTL CIFIST atmospheric models (Baraffe et al. 2015) in the fit, both to estimate the $T_{\rm eff}$ and fill in gaps in the template spectra (e.g., beyond 2.3$\mu$m). We integrated the resulting absolutely-calibrated spectrum to estimate the bolometric flux ($F_{\rm bol}$), which we combined with the *G*aia EDR3 parallax to estimate the stellar luminosity ($L_*$). With $T_{\rm eff}$ and $L_*$, we calculated $R_*$ using the Stefan-Boltzmann relation. While reddening in this sight-line is low (Schlafly & Finkbeiner 2011), KOI-3876 is well outside the Local Bubble, so we included extinction as part of the fit. To account for variability in the star, we added (in quadrature) 0.02 mags to the errors of all optical photometry. In total, the fit included six free parameters: the spectral template, $A_V$, three parameters that describe the model ($log\ g$, $T_{\rm eff}$, and [M/H]), and a scale factor between the model and the photometry. We show an example fit in Figure 9.

For KOI-3876, the resulting fit yielded $A_V = 0.16^{+0.10}_{-0.08}$, $T_{\rm eff}$=5672 ± 65 K, $F_{\rm bol}$=(2.55 ± 0.10) × 10$^{-10}$ (erg cm$^{-2}$ s$^{-1}$), $L_* = 0.81 \pm 0.03L_\odot$, and $R_* = 0.94 \pm 0.03R_\odot$. For Kepler-970, we found $A_V = 0.28 \pm 0.12$, $T_{\rm eff}$=4290 ± 70 K, $F_{\rm bol}$=(4.88 ± 0.23) × 10$^{-11}$ (erg cm$^{-2}$ s$^{-1}$), $L_* = 0.168 \pm 0.010L_\odot$, and $R_* = 0.715 \pm 0.03R_\odot$.

Our SED parameters were in good agreement with the literature spectroscopic values for both stars. Since KOI-3876 is Sun-like, we considered the high-resolution spectroscopic $T_{\rm eff}$ to be more reliable than the SED-based value, but the SED-based luminosity (and radius) more reliable than one derived from the spectroscopic $log\ g$ or isochrone. We combined the two, which yielded a final radius of $0.92 \pm 0.02R_\odot$. For Kepler-970, we adopted our SED-fit parameters for all values.

### 6.3. *Stellar mass*

To determine $M_*$ for KOI-3876, we compared the observed photometry to Solar-metallicity magnetic DSEP evolution models and PARSEC models. We used `emcee` to simultaneously fit for age, $A_V$, $M_*$, and an additional parameter to capture underestimated uncertainties in the data or models ($f$, in magnitudes) within an MCMC framework. We used a hybrid interpolation method, first identifying the nearest age in then model grid and then performing a linear interpolation in mass to obtain stellar parameters and model photometry. Since this method could not interpolate between

**Table 2.** Planetary Candidates in MELANGE-2.

| ID | Disposition | Membership | Period (days) | T0 (BJD) | Depth (ppm) |
|---|---|---|---|---|---|
| KOI-678.01 | Confirmed | N | 6.040 | 2455005.594 | 241 |
| KOI-678.02 | Confirmed | N | 4.139 | 2454965.016 | 256 |
| KOI-966.01 | EB | Y | 0.379 | 2455003.248 | 1973 |
| KOI-966.02 | EB | Y | 7.769 | 2454966.090 | 1730 |
| KOI-1838.01 | Confirmed | Y | 16.736 | 2454976.132 | 1147 |
| KOI-5304.01 | FP | N | 206.310 | 2455064.818 | 277 |
| KOI-6819.01 | Candidate | N | 3.226 | 2454967.419 | 36 |
| KOI-7059.01 | EB | N | 31.973 | 2454966.867 | 75053 |
| KIC 6366739 | Low SNR | N | 22.321 | 2455386.607 | 2277 |
| TIC 20352534 | Candidate | N | 6.377 | 2458687.871 | 5852 |
| TIC 237181417 | Candidate | N | 10.870 | 2458690.562 | 3178 |
| TIC 272486188 | Rejected | N | 9.040 | 2458683.604 | 779 |
| TIC 28768382 | Candidate | N | 11.790 | 2458692.723 | 1430 |
| TIC 138966713 | Candidate | Y | 19.701 | 2458687.657 | 1858 |
| TIC 158168145 | Candidate | Y | 7.107 | 2458689.709 | 1908 |
| TIC 158415341 | Rejected | N | 20.016 | 2458690.503 | 7571 |
| TIC 164678171 | Rejected | N | 12.392 | 2458695.552 | 1277 |
| TIC 355909811 | Candidate | N | 6.065 | 2458686.931 | 10753 |

ages, we re-sampled the input grid using the `isochrones` package (Morton 2015a) to be more dense (0.1 Myr and $0.01 M_\odot$) than expected errors. To redden the model photometry, we used `synphot` (Lim 2020) and the extinction law from Cardelli et al. (1989). We placed a Gaussian prior on age of $105\pm10$ Myr, while other parameters evolved under uniform priors. The resulting fit from each model grid was very precise, but differences between the two grids suggest larger systematic errors. Considering these, the resulting parameters were generally in agreement with our spectroscopic constraints ($R_* = 0.968\pm0.07$, $A_V = 0.27\pm0.10$, $T_{\rm eff}=5710\pm60$) and provided a stellar mass estimate of $M_* = 1.04\pm0.03 M_\odot$. We combined this with our earlier radius estimate to get an estimate of the stellar density ($\rho_* = 1.30\pm0.10\rho_\odot$).

Kepler-970 is low-mass enough to fit within the bounds of the $M_K-M_*$ relation from Mann et al. (2019). We used the *Gaia* EDR3 parallax with uncertainties corrected for underestimated errors following El-Badry et al. (2021) and the 2MASS $K_S$ magnitude. We applied a correction for reddening based on our SED fit (Section 6.2), although this was negligible in $K_S$ band compared to other uncertainties. We fed the resulting values into the fit posteriors using the provided code[4], which yielded a mass of $0.66 \pm 0.02 M_\odot$. Combining with the radius above, this gives a stellar density of $1.88\pm0.24\rho_\odot$.
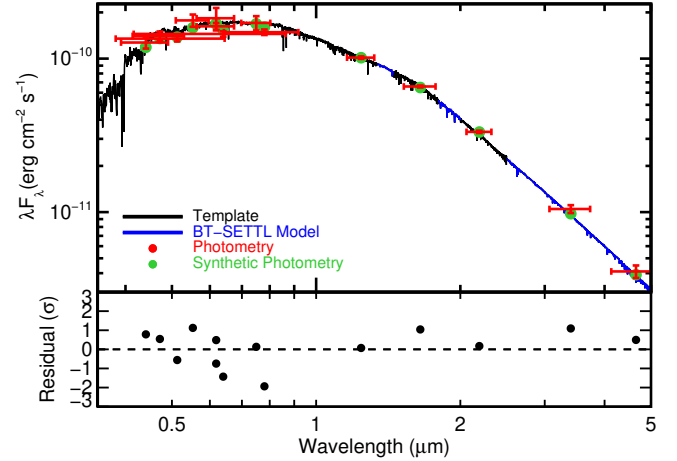
[4] https://github.com/awmann/M_-M_K-



**Figure 9.** Best-fit template spectrum (G1V; black) and synthetic photometry (green) compared to the observed photometry of KOI-3876 (red). Errors on observed photometry are shown as vertical error bars, while horizontal error bars indicate the approximate width of the filter. BT-SETTL models (blue) were used to fill in regions of high telluric absorption or beyond the template range. The bottom panel shows the photometric residual in units of standard deviations.

### 6.4. *Stellar inclination*

To test whether the stellar spin and planetary orbit are consistent with alignment, we computed the stellar inclination ($i_*$) from the $v\sin i_*$, $P_{\rm rot}$, and $R_*$ values estimated above. In is simplest form, this calculation is

**Table 3.** Properties of KOI-3876 and Kepler-970

| Parameter | KOI-3876 | Kepler-970 | Source |
|---|---|---|---|
| | | Name | |
| Gaia EDR3 | 2052827207364859264 | 2101379205604338688 | Gaia Collaboration et al. (2021) |
| KOI | 3876 | 1838 | Twicken et al. (2016) |
| KIC | 3440118 | 5526527 | Brown et al. (2011) |
| TIC | 122450696 | 122069243 | Stassun et al. (2018) |
| 2MASS | J19214575+3831248 | J19183005+4042314 | Skrutskie et al. (2006) |
| | | Astrometry | |
| $\alpha$ | 290.440629 | 289.625218 | *Gaia* EDR3 |
| $\delta$. | 38.523572 | 40.708735 | *Gaia* EDR3 |
| $\mu_\alpha$ (mas yr$^{-1}$) | -4.154±0.010 | -2.739±0.020 | *Gaia* EDR3 |
| $\mu_\delta$ (mas yr$^{-1}$) | 2.269±0.011 | 1.652±.024 | *Gaia* EDR3 |
| $\pi$ (mas) | 3.0565±0.0093 | 3.0153±0.0186 | *Gaia* EDR3 |
| | | Photometry | |
| $G_{Gaia}$ (mag) | 12.6054±0.0028 | 14.7876±0.0029 | *Gaia* EDR3 |
| $BP_{Gaia}$ (mag) | 12.9642±0.0033 | 5.4884±0.0049 | *Gaia* EDR3 |
| $RP_{Gaia}$ (mag) | 12.0798±0.0041 | 13.9759±0.0048 | *Gaia* EDR3 |
| $B$ (mag) | 13.375 ± 0.094 | ... | APASS |
| $V$ (mag) | 12.655 ± 0.122 | ... | APASS |
| $g'$ (mag) | 13.038 ± 0.033 | ... | APASS |
| $r'$ (mag) | 12.456 ± 0.092 | ... | APASS |
| $i'$ (mag) | 12.323 ± 0.062 | ... | APASS |
| $J$ (mag) | 11.456 ± 0.02 | 12.980±0.023 | 2MASS |
| $H$ (mag) | 11.152 ± 0.016 | 12.355±0.023 | 2MASS |
| $K_S$ (mag) | 11.107 ± 0.019 | 12.215±0.022 | 2MASS |
| $W1$ (mag) | 11.06 ± 0.023 | 12.155±0.022 | ALLWISE |
| $W2$ (mag) | 11.09 ± 0.020 | 12.193±0.022 | ALLWISE |
| $W3$ (mag) | 10.91 ± 0.094 | 12.195±0.282 | ALLWISE |
| | | Kinematics & Position | |
| RV$_{Bary}$ (km s$^{-1}$) | -26.79±0.01 | -27.15±0.10 | Jönsson et al. (2020); Petigura (in prep) |
| U (km s$^{-1}$) | -9.467 ± 0.016 | -8.815 ± 0.047 | This work |
| V (km s$^{-1}$) | -26.034 ± 0.012 | -26.146 ± 0.092 | This work |
| W (km s$^{-1}$) | 2.048 ± 0.032 | -1.034 ± 0.055 | This work |
| X (pc) | 105.98 ± 0.42 | 97.55 ± 0.78 | This work |
| Y (pc) | 303.03 ± 1.20 | 308.66 ± 2.45 | This work |
| Z (pc) | 62.86 ± 0.25 | 72.28 ± 0.58 | This work |
| | | Physical Properties | |
| $P_{\rm rot}$ (days) | 4.69 ± 0.04 | 9.23 ±0.66 | Nielsen et al. (2013); Santos et al. (2019) |
| $v \sin i_*$ (km s$^{-1}$) | 10.4 ± 0.5 | 5.2±1.0km s$^{-1}$ | Brewer & Fischer (2018); Petigura (in prep) |
| $i_*$ (°) | > 80 | > 52 | This work |
| $F_{\rm bol}$ (erg cm$^{-2}$ s$^{-1}$) | $(2.55 ± 0.10) \times 10^{-10}$ | $(4.88 ± 0.23) \times 10^{-11}$ | This work |
| $T_{\rm eff}$ (K) | 5720 ± 60 | 4290 ± 70 | CKS; This work |
| [Fe/H] | 0.12 ± 0.02 | 0.04±0.09 | Brewer & Fischer (2018); Petigura (in prep) |
| M$_\star$ (M$_\odot$) | 1.01 ± 0.03 | 0.67±0.02 | This work |
| R$_\star$ (R$_\odot$) | 0.92 ± 0.02 | 0.71 ± 0.03 | This work |
| L$_\star$ (L$_\odot$) | 0.81 ± 0.03 | 0.168 ± 0.010 | This work |
| $\rho_\star$ ($\rho_\odot$) | 1.30 ± 0.10 | 1.88±0.24 | This work |
| Age (Myr) | 105 ± 10 | | This work |

$V = 2\pi R_*/P_{\rm rot}$, but requires additional statistical corrections (see Morton & Winn 2014; Masuda & Winn 2020). Here we followed the methodology described in Masuda & Winn (2020). For KOI-3876, the resulting stellar inclination was $i_* > 71°$ at 95% confidence and $i_* > 80°$ at 68% confidence. For Kepler-970, the values were $i_* > 52°$ and $i_* > 70°$ at 95% and 68%, respectively. Both are consistent with alignment with the orbital inclinations.

## 7. TRANSIT PARAMETERS

We fit the *Kepler* photometry using the misttborn (MCMC Interface for Synthesis of Transits, Tomography, Binaries, and Others of a Relevant Nature) fitting

code[5] first described in Mann et al. (2016a) and expanded upon in Johnson et al. (2018). misttborn uses BATMAN (Kreidberg 2015) to generate model light curves and emcee (Foreman-Mackey et al. 2013) to explore the transit parameter space.

The standard implementation of misttborn fits for six parameters for each transiting planet: time of periastron ($T_0$), orbital period of the planet ($P$), planet-to-star radius ratio ($R_p/R_\star$), impact parameter ($b$), and stellar density ($\rho_\star$). We fit two linear and quadratic limb-darkening coefficients ($q_1$, $q_2$) following the triangular sampling prescription of Kipping (2013).

We ran two versions of the fit. In the first, the MCMC chain restricted $e$ to 0 and allowed $\rho_\star$ to vary within a uniform distribution, and the second allowed $e$ to vary with a Gaussian prior on $\rho_\star$ from our spectroscopic and SED analysis (Section 6). For both fits, applied Gaussian priors on the limb-darkening coefficients based on the values derived using our stellar parameters from Section 6 and the LDTK toolkit Parviainen & Aigrain (2015), with errors accounting for the difference between models: $g_1 = 0.42 \pm 0.08$, $g_2 = 0.13 \pm 0.04$ for KOI3876 and $g_1 = 0.51 \pm 0.08$, $g_2 = 0.13 \pm 0.04$ for Kepler-970. Other transit parameters were sampled uniformly with physically motivated boundaries; e.g., $T_0$ was restricted to the time period sampled by the data, $|b| < 1 + R_P/R_*$, $0 < e < 1$, $0 < \rho_*$, and $0 < R_P/R_* < 1$.

To model stellar variations, misttborn includes a Gaussian Process (GP) regression module, utilizing the celerite code (Foreman-Mackey et al. 2017). We initially used a mixture of two stochastically driven damped simple harmonic oscillators (SHOs) at periods $P_{GP}$ (primary) and $0.5P_{GP}$ (secondary), as is common for fitting stellar variability. However, we found that for both planets, the second SHO was not required (the model was weighting it to zero), and re-ran with a single SHO. There were three GP parameters: the log of the GP period ($\ln(P_{GP})$), the log of the GP amplitude ($\ln$ Amp), and a decay timescale for the variability (quality factor, $\ln Q$). We used a weak Gaussian prior (20%) on the GP period to keep walkers from wandering to half and double aliases. All other GP parameters evolved under uniform priors.

For each of the four runs (two planets each with and without eccentricity), we ran the MCMC using 50 walkers for 250,000 steps including a burn-in of 20,000 steps. The total run was more than 50 times the autocorrelation time (for all fits), indicating that the total run was sufficient for convergence.

As we show in Figures 10, the SHO GP fits did an excellent job describing the overall variability for both planets, even in the presence of complex changes in the light curve morphology over 4.5 years of observations by *Kepler*. We also show the phase folded light curves in Figure 11 for the fit where $e$ was allowed to vary. The best-fit parameters with uncertainties for both fits can be found in Table 4, and the corner plot for the major transit-fit parameters for the eccentric fits are in Figure 12.

For KOI-3876 and Kepler-970, the first fit ($e = 0$) yielded a $\rho_\star$ value larger than the spectroscopic/isochronal value determined in Section 6 ($15.5\rho_\odot$ vs $1.3\rho_\odot$ and $15.2\rho_\odot$ vs $1.9\rho_\odot$). Although the error on the transit-fit density is large ($5.9\rho_\odot$ and $6.7\rho_\odot$), so the two values were consistent at $\simeq 2.5\sigma$. But it is suggestive that the planets are on eccentric orbits. Indeed, in the fits where $e$ is allowed to float, the highest-likelihood models had $e \gtrsim 0.3$ for both planets. For this reason, we prefer the fit where $e$ was allowed to float for both targets.

### 7.1. *False Positive Analysis*

In Morton et al. (2016), the authors run the false-positive probability calculator VESPA Morton (2015b) on all *Kepler* objects of interest available at the time, which included both KOI-3876 b and Kepler-970 b. Kepler-970 b was validated as planetary, and a qualitative inspection of the light curve and archival data re-affirms this conclusion. The light curve has the expected shape, there are no visible companions in the high-resolution imaging, and the nearest star detected in *G*aia imaging ($\simeq 4''$ away) is too faint to reproduce the transit depth and shape. We do not revisit this assessment.

However, Morton et al. (2016) assigned a high probability (90%) that the signal associated with KOI-3876 b is an eclipsing binary and a $< 1\%$ probability that the signal is due to a planet. This conclusion was based primarily on the light curve morphology and available stellar parameters.

As we show in Figure 13, radial velocities from the Apache Point Observatory Galactic Evolution Experiment 16th data release (APOGEE DR16; Jönsson et al. 2020) rule out any stellar companion at the period of the planet. Further, our light curve analysis shows the expected U-shape transit for a planet, and there is no sign of a companion in the extant spectroscopy or adaptive optics imaging and non-redundant aperture masking from Kraus et al. (2016). *G*aia EDR3 astrometry and imaging similarly shows no sign of a compan-

**Table 4.** Parameters of KOI-3876 and Kepler-970

| Parameter | KOI-3876 | | Kepler-970 | |
|---|---|---|---|---|
| | e=0 | e float (preferred) | e=0 | e float (preferred) |
| Measured Parameters | | | | |
| $T_0$ (BJD-2454833) | $131.71488 \pm 0.00088$ | $131.71484^{+0.00093}_{-0.00092}$ | $143.13258^{+0.00099}_{-0.00098}$ | $143.1326 \pm 0.0011$ |
| $P$ (days) | $19.577831 \pm 2.1 \times 10^{-5}$ | $19.57783 \pm 2.1 \times 10^{-5}$ | $16.736525 \pm 2 \times 10^{-5}$ | $16.736525 \pm 2 \times 10^{-5}$ |
| $R_P/R_\star$ | $0.01945^{+0.00061}_{-0.00044}$ | $0.01977^{+0.00116}_{-0.00063}$ | $0.03186^{+0.00136}_{-0.00077}$ | $0.0337^{+0.0031}_{-0.0022}$ |
| $b$ | $0.31^{+0.28}_{-0.22}$ | $0.51^{+0.27}_{-0.33}$ | $0.33^{+0.3}_{-0.23}$ | $0.7^{+0.18}_{-0.44}$ |
| $\rho_\star$ ($\rho_\odot$) | $15.5^{+2.5}_{-5.9}$ | $1.305^{+0.096}_{-0.093}$ | $15.2^{+2.9}_{-6.7}$ | $1.882^{+0.09}_{-0.088}$ |
| $q_{1,1}$ | $0.289^{+0.107}_{-0.1}$ | $0.294^{+0.104}_{-0.094}$ | $0.37 \pm 0.12$ | $0.38 \pm 0.12$ |
| $q_{2,1}$ | $0.371^{+0.075}_{-0.086}$ | $0.375^{+0.073}_{-0.087}$ | $0.374^{+0.07}_{-0.078}$ | $0.376^{+0.071}_{-0.076}$ |
| $\sqrt{e}\sin\omega$ | – | $0.42^{+0.16}_{-0.31}$ | – | $0.25^{+0.25}_{-0.3}$ |
| $\sqrt{e}\cos\omega$ | – | $-0.06^{+0.6}_{-0.58}$ | – | $-0.0^{+0.55}_{-0.54}$ |
| $\log(P_{GP})$ | $1.495^{+0.016}_{-0.014}$ | $1.495^{+0.016}_{-0.015}$ | $2.839^{+0.056}_{-0.053}$ | $2.838^{+0.056}_{-0.051}$ |
| $\log(Amp)$ | $-9.338^{+0.057}_{-0.055}$ | $-9.338^{+0.058}_{-0.054}$ | $-6.797^{+0.079}_{-0.075}$ | $-6.799^{+0.078}_{-0.076}$ |
| $\log(Q)$ | $1.154^{+0.058}_{-0.055}$ | $1.154^{+0.061}_{-0.054}$ | $0.664^{+0.029}_{-0.025}$ | $0.665^{+0.027}_{-0.025}$ |
| Derived Parameters | | | | |
| $a/R_\star$ | $76.2^{+3.9}_{-10.0}$ | $48.0^{+3.3}_{-6.7}$ | $68.2^{+4.0}_{-10.0}$ | $42.2^{+6.5}_{-7.6}$ |
| $i$ (°) | $89.76^{+0.17}_{-0.29}$ | $88.99^{+0.65}_{-0.45}$ | $89.72^{+0.2}_{-0.37}$ | $88.74^{+0.77}_{-0.26}$ |
| $T_{14}$ (days) | $0.0793^{+0.0016}_{-0.0015}$ | $0.106^{+0.071}_{-0.033}$ | $0.0763^{+0.0021}_{-0.0018}$ | $0.09^{+0.047}_{-0.023}$ |
| $T_{23}$ (days) | $0.0755^{+0.0015}_{-0.0016}$ | $0.099^{+0.067}_{-0.032}$ | $0.0703^{+0.0019}_{-0.0024}$ | $0.075^{+0.046}_{-0.022}$ |
| $R_P$ ($R_\oplus$) | $1.953^{+0.075}_{-0.061}$ | $1.985^{+0.124}_{-0.077}$ | $2.467^{+0.148}_{-0.149}$ | $2.609^{+0.265}_{-0.203}$ |
| $a$ (AU) | $0.313^{+0.046}_{-0.064}$ | $0.197^{+0.031}_{-0.039}$ | $0.225^{+0.016}_{-0.041}$ | $0.139^{+0.022}_{-0.026}$ |
| $e$ | … | $0.42^{+0.18}_{-0.13}$ | … | $0.34^{+0.18}_{-0.22}$ |
| $\omega$ (°) | … | $102.0 \pm 62.0$ | … | $117.0^{+75.0}_{-85.0}$ |

ion. There is only one star detected with the *Kepler* PSF, which is too faint to reproduce the transit. KOI-3876 also has a low Renormalised Unit Weight Error (RUWE) in EDR3 (0.94). RUWE value is effectively an astrometric reduced $\chi^2$ value, normalized to correct for color and brightness dependent effects[6]. RUWE should be around 1 for well-behaved sources, and higher values (RUWE$\gtrsim$1.3) suggests with the presence of a stellar companion (Ziegler et al. 2020; Wood et al. 2021).

It is possible the high Morton et al. (2016) was an artifact of poor detrending of the high stellar variability in KOI-3876 and/or the mismatch between the transit duration and that expected for a circular orbit (see Section 7). So we re-ran the VESPA analysis using our GP-detrended curve and the updated imaging constraints. We found a 97% probability KOI-3876 b is a planet and a 3% probability KOI-3876 b is an eclipsing binary. Other false-positive scenarios (background EB and hierarchical EB) had negligible < 0.1% probabilities. As previously stated and shown in Figure 13, the APOGEE velocities rule out a stellar companion to KOI-3876 at the period of the planet. Including the velocities is more than suf-

ficient to statistically validate the signal as planetary in origin.

## 8. SUMMARY AND CONCLUSIONS

KOI-3876 b and Kepler-970 b are transiting planets discovered by the *Kepler* mission inside a young stellar association. We initially identified the association as an overdensity of stars in Galactic positions and tangential velocities around KOI-3876. Through member rotation periods, lithium abundances, and a comparison to model isochrones, we show the collection of stars is co-eval, with an age similar to that of Pleiades ($\simeq 110$ Myr). We refer to this group as MELANGE-2, although a comparison suggests it is likely one part of the known Theia 316 string (Kounkel & Covey 2019; Kounkel et al. 2020).

Interestingly, even among our high-probability members of MELANGE-2, more than half are missing from the Theia 316 list. Similarly, our list only contains one branch of Theia 316. In combination, this suggests the structure has far more stars than even the combination of the two lists. A more detailed analysis with *TESS* rotations and *Gaia* DR3 velocities would be invaluable here, and for the thousands of other candidate associations identified by Kounkel et al. (2020); Kounkel & Covey (2019) and others.

---

[6] https://gea.esac.esa.int/archive/documentation/GDR2/Gaia_archive/chap_datamodel/sec_dm_main_tables/ssec_dm_ruwe.html
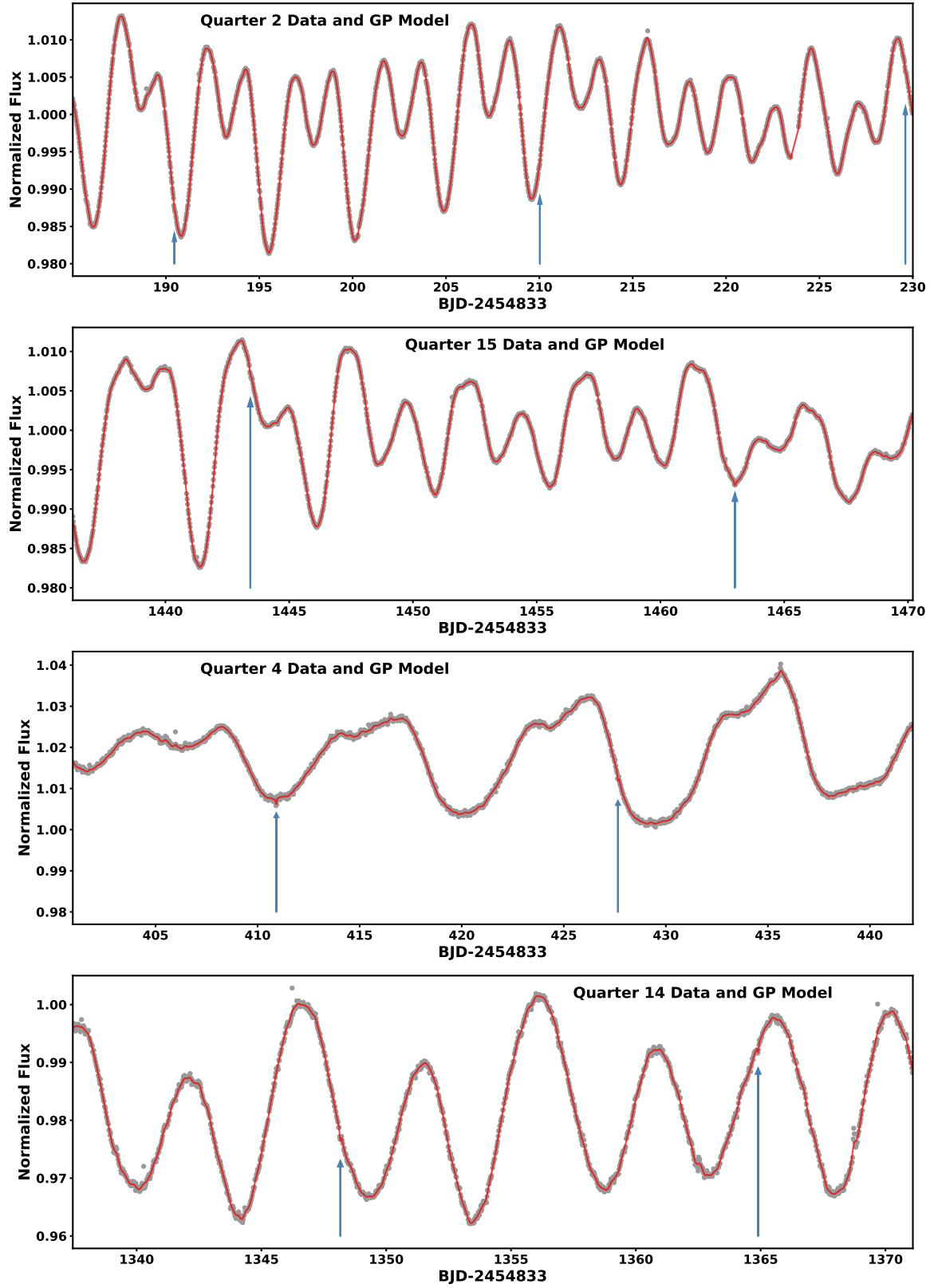
BARBER ET AL.



**Figure 10.** Representative sections of the two planet host light curves. The top two are for KOI-3876, while the bottom two are for Kepler-970. The grey points are the *Kepler* data, the red line shows the best-fit GP model, and the arrows indicate transits.
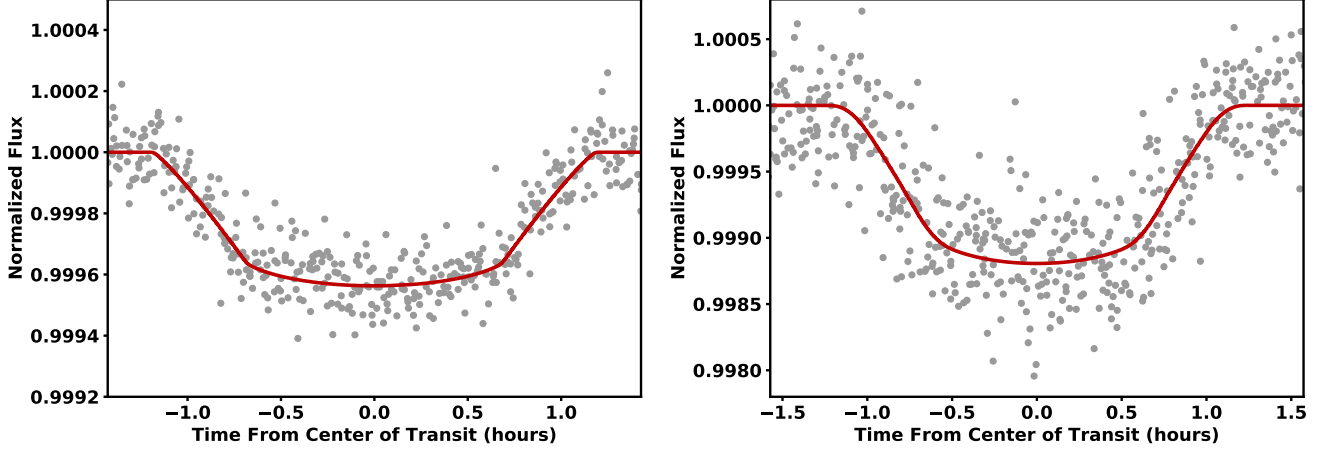
**Figure 11.** Phase-folded light curve of KOI-3876 (left) and Kepler-970 (right) from *Kepler* (grey points) with the best-fit transit model (red). The best-fit GP model to the stellar variability has been removed from both the data and the model for clarity. Both planets show the expected transit shape.
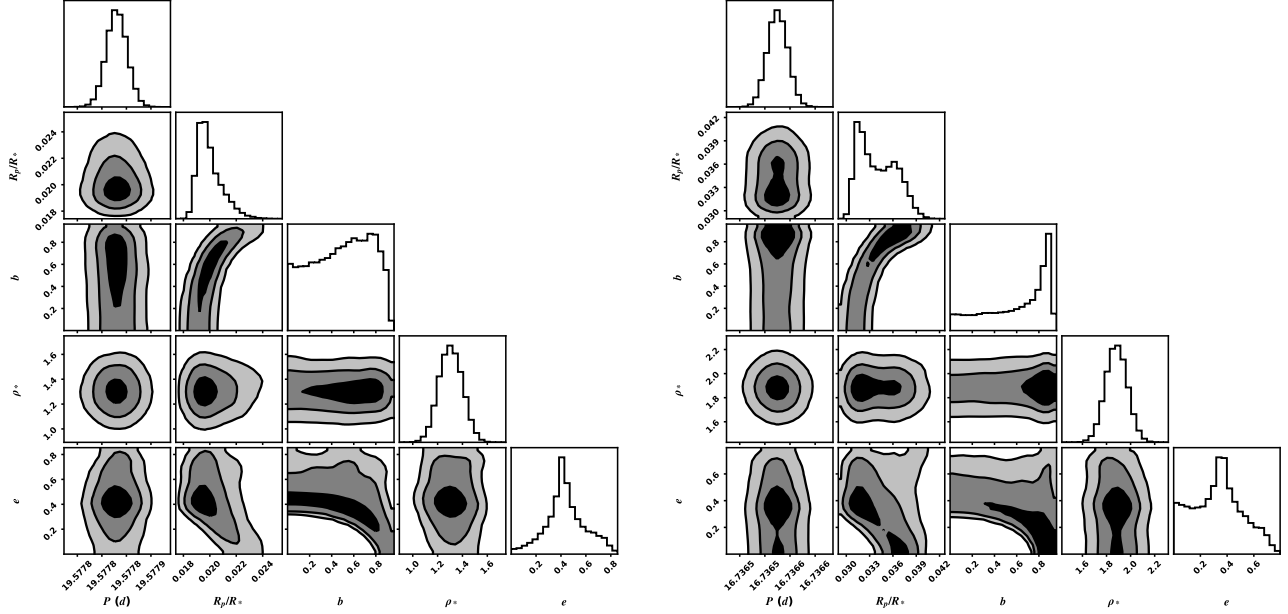


**Figure 12.** Corner plot of the major transit parameters ($P$, $R_P/R_*$, $b$, $\rho_*$, and $e$) from our `MISTTBORN` fit for KOI-3876 b (left) and Kepler-970 b (right). The contour levels correspond to $1\sigma$, $2\sigma$, and $3\sigma$ of the points (from darkest to lightest). The planet-to-star radius ratio and eccentricity are strongly covariant with impact parameter, as a higher impact parameter requires a deeper transit (and lower eccentricity) to reproduce the observed transit depth (and duration). It is difficult to break this degeneracy with *Kepler* long-cadence data alone, as the integration time is longer than the ingress/egress. Plot made using corner.py (Foreman-Mackey 2016).

Taking into account the updated (younger) age and utilizing new methods for analyzing variable light curves, we update the stellar and transit parameters for KOI-3876 b. We find KOI-3876 b to be about twice the size of the earth, orbiting a young analog to the Sun every 19.577 days. The transit duration also suggests a modest eccentricity, although errors are too large to rule out a circular orbit. Although Morton et al. (2016) pre-

viously found KOI-3876 b was likely an eclipsing binary, we rule out this disposition based on APOGEE radial velocities and our own light curve analysis and validate the signal as planetary in origin. The residual velocities are too small to be due to a stellar-mass companion, and the unexplained jitter is likely due to the stellar jitter that is common in young stars since the variation is still below expected for even a tight eclipsing binary.
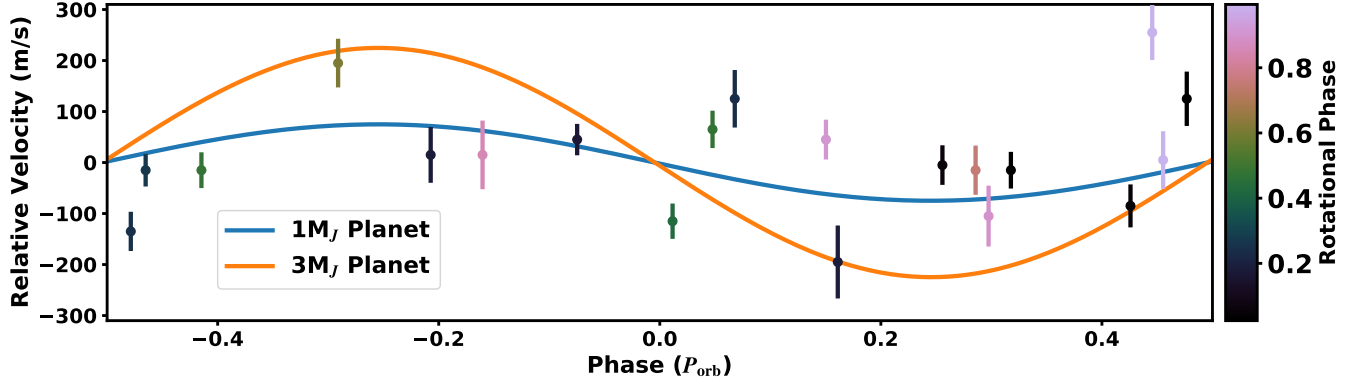
**Figure 13.** Radial velocities from APOGEE (Jönsson et al. 2020) for KOI-3876 as a function of the planet's orbital phase and colored by the rotational phase. The velocities rule out any companion more massive than $\simeq 2M_J$, ruling out any possibility of an eclipsing binary at the transit period. The scatter is larger than expected for the uncertainties by $\simeq 100\,\mathrm{m\,s^{-1}}$, most likely due to stellar jitter common in young stars (Brems et al. 2019; Tran et al. 2021). The residual jitter is still far below the expected variation for a tight eclipsing binary.

Kepler-970 b was previously validated as a planet (Morton et al. 2016). As with KOI-3876 b we update the stellar and planet parameters using the new younger age. We find Kepler-970 b to be about $2.5R_\oplus$, orbiting a young K dwarf every 16.74 days. The transit was previously shown to exhibit transit timing variations (TTVs; e.g., Ford et al. 2012; Holczer et al. 2016). Unfortunately, the period of the variation is $\simeq 2000$ days, and we did not detect a transit for the outer perturber. Thus, we could not further constrain the system from the TTVs. Our fit assumed a linear ephemeris, which can lead to a distortion in the transit in the presence of a TTV (a shallower depth and longer duration, e.g., Mann et al. 2017a). However, the TTV amplitude is small ($\lesssim 10$ m Holczer et al. 2016), and our transit parameters are generally consistent earlier analyses.

We searched for additional candidates in MELANGE-2. Although we identify many candidates and recover some known KOIs (see Table 2), most of these were either not real members, false positives, or did not meet our threshold for significance. Ultimately, only KOI-3876 b and Kepler-970 b passed all tests. Additional *TESS* data on the *Kepler* field, as well as a more complete census of the Theia 316 group might yield more candidates in the future.

These two planets join the growing number of young transiting planets, which we show in Figure 14. KOI-3876 b and Kepler-970 b land in the heavily populated region of mini-Neptunes. The infant (10-50 Myr) planets that tend to land between Neptune and Jupiter due to a combination of radius evolution (Mann et al. 2017b; Owen 2020) and sensitivity variations with age (Rizzuto et al. 2017).

Stellar angular momentum and rotationally driven magnetic activity are both age and mass dependent. Ro-
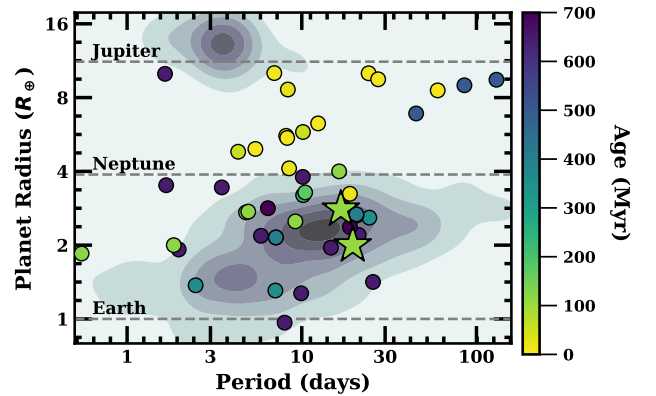


**Figure 14.** The current census of young (Hyades-age or younger) transiting planets. Points are color-coded by age. The two stars are KOI-3876 b and Kepler-970 b. The contours represent the density of (mostly older) transiting planets from *Kepler*. Planet parameters taken from the NASA exoplanet archive (NASA Exoplanet Science Institute 2020).

tation periods in open clusters are useful for studying these phenomena, but there is a lack of low-mass ($< 0.5$ $M_\odot$) rotation periods available (Covey et al. 2016). Rebull et al. (2016a) seeks to help alleviate this problem, contributing 500 new rotation periods for Pleiades members, with a focus on the low-mass end. This work calculates rotation periods for 76 targets in the MELANGE-2 population. 49 are K-type or M-type stars, which are more likely to be within this low-mass boundary, with rotation periods ranging from 0.16 to 14.9 days. Further work on the analysis of the distribution of rotation periods versus color can be done and extend the sample size used in analyses, such as in Rebull et al. (2016b).

The long baseline of *Kepler* has enabled studies of spot lifetime (e.g., Giles et al. 2017). For example, starspots

have shorter lifetimes on stars with faster rotation periods (Basri et al. 2022). This is likely due to age, i.e., that younger stars have shorter spot lifetimes. MELANGE-2 and the younger $\delta$-Lyr cluster (Bouma et al. 2021) have enough overlap with the *Kepler* field for a more direct test of how spot lifetimes (among other properties) vary with age.

Recent searches found no transiting planets in the $K2$ data of the similar-aged Pleiades cluster (Gaidos et al. 2017; Rizzuto et al. 2017). Gaidos et al. (2017) argue this deficit is not surprising given our sensitivity to planets in Pleiades, although the more effective transit-search methods of Rizzuto et al. (2017) suggest more tension with the field. The difference depends on details of the planet and stellar populations. The discovery of TOI-451 bcd in the $\simeq$120 Myr Psc-Eri cluster (Newton et al. 2021) and the planets in this work favor the former. Inspection of the sensitivity results results from Rizzuto et al. (2017) suggest the planets here would have landed just below the detection limits from the $K2$ data of similar stars in the Pleiades.

We have known there are young planet-hosts in the *Kepler* field from their rotation periods (Walkowicz & Basri 2013; David et al. 2021) and lithium levels (Berger et al. 2018). But such ages are generally imprecise outside a co-eval association. The previous challenge for *Kepler* was the lack of young associations in the field. MELANGE-2 as well as the recently identified $\delta$-Lyr cluster (Bouma et al. 2021) demonstrate that the list of four known clusters in the *Kepler* field was incomplete and motivates the work for more in the *Kepler* $K2$ and CoRoT (Auvergne et al. 2009) fields. In addition to surveys like Theia Kounkel & Covey (2019); Kounkel et al. (2020), the methods applied here may reveal a huge population of young associations harboring known transiting systems.

*Facilities:* TESS, Kepler, Gaia, Sloan (APOGEE), Smith (Coude)

*Software:* `misttborn.py` (Johnson et al. 2018), `galpy` (Bovy 2015), *emcee* (Foreman-Mackey et al. 2013), *batman* (Kreidberg 2015), matplotlib (Hunter 2007), `corner.py` (Foreman-Mackey 2016), `Celerite` (Foreman-Mackey et al. 2017)

## REFERENCES

Aigrain, S., Llama, J., Ceillier, T., et al. 2015, MNRAS, 450, 3211, doi: 10.1093/mnras/stv853

Anguiano, B., Majewski, S. R., Allende Prieto, C., et al. 2018, A&A, 620, A76, doi: 10.1051/0004-6361/201833387

Angus, R., Aigrain, S., Foreman-Mackey, D., & McQuillan, A. 2015, MNRAS, 450, 1787, doi: 10.1093/mnras/stv423

Auvergne, M., Bodin, P., Boisnard, L., et al. 2009, A&A, 506, 411, doi: 10.1051/0004-6361/200810860

Baraffe, I., Homeier, D., Allard, F., & Chabrier, G. 2015, A&A, 577, A42, doi: 10.1051/0004-6361/201425481

Barnes, S. A. 2007, ApJ, 669, 1167, doi: 10.1086/519295

Basri, G., Streichenberger, T., McWard, C., et al. 2022, ApJ, 924, 31, doi: 10.3847/1538-4357/ac3420

Batalha, N. M., Borucki, W. J., Koch, D. G., et al. 2010, ApJL, 713, L109, doi: 10.1088/2041-8205/713/2/L109

Berger, T. A., Howard, A. W., & Boesgaard, A. M. 2018, ApJ, 855, 115, doi: 10.3847/1538-4357/aab154

Berger, T. A., Huber, D., van Saders, J. L., et al. 2020, AJ, 159, 280, doi: 10.3847/1538-3881/159/6/280

Bochanski, J. J., Munn, J. A., Hawley, S. L., et al. 2007, AJ, 134, 2418, doi: 10.1086/522053

Bouma, L. G., Hartman, J. D., Bhatti, W., Winn, J. N., & Bakos, G. Á. 2019, ApJS, 245, 13, doi: 10.3847/1538-4365/ab4a7e

Bouma, L. G., Curtis, J. L., Masuda, K., et al. 2021, arXiv e-prints, arXiv:2112.14776. https://arxiv.org/abs/2112.14776

Bouvier, J., Barrado, D., Moraux, E., et al. 2018, A&A, 613, A63, doi: 10.1051/0004-6361/201731881

Bovy, J. 2015, ApJS, 216, 29, doi: 10.1088/0067-0049/216/2/29

Bovy, J., & Hogg, D. W. 2010, ApJ, 717, 617, doi: 10.1088/0004-637X/717/2/617

Brems, S. S., Kürster, M., Trifonov, T., Reffert, S., & Quirrenbach, A. 2019, A&A, 632, A37, doi: 10.1051/0004-6361/201935520

Bressan, A., Marigo, P., Girardi, L., et al. 2012, MNRAS, 427, 127, doi: 10.1111/j.1365-2966.2012.21948.x

Brewer, J. M., & Fischer, D. A. 2018, ApJS, 237, 38, doi: 10.3847/1538-4365/aad501

Brown, T. M., Latham, D. W., Everett, M. E., & Esquerdo, G. A. 2011, AJ, 142, 112, doi: 10.1088/0004-6256/142/4/112

Cardelli, J. A., Clayton, G. C., & Mathis, J. S. 1989, ApJ, 345, 245, doi: 10.1086/167900

Corsaro, E., Stello, D., Huber, D., et al. 2012, ApJ, 757, 190, doi: 10.1088/0004-637X/757/2/190

Coughlin, J. L., Mullally, F., Thompson, S. E., et al. 2016, ApJS, 224, 12, doi: 10.3847/0067-0049/224/1/12

Covey, K. R., Agüeros, M. A., Law, N. M., et al. 2016, ApJ, 822, 81, doi: 10.3847/0004-637X/822/2/81

Cummings, J. D., Deliyannis, C. P., Maderak, R. M., & Steinhauer, A. 2017, AJ, 153, 128, doi: 10.3847/1538-3881/aa5b86

Curtis, J. L., Agüeros, M. A., Douglas, S. T., & Meibom, S. 2019, ApJ, 879, 49, doi: 10.3847/1538-4357/ab2393

Cutri, R. M., & et al. 2014, VizieR Online Data Catalog, II/328

Dahm, S. E. 2015, ApJ, 813, 108, doi: 10.1088/0004-637X/813/2/108

David, T. J., Contardo, G., Sandoval, A., et al. 2021, AJ, 161, 265, doi: 10.3847/1538-3881/abf439

Dotter, A., Chaboyer, B., Jevremović, D., et al. 2008, ApJS, 178, 89, doi: 10.1086/589654

Douglas, S. T., Agüeros, M. A., Covey, K. R., & Kraus, A. 2017, ApJ, 842, 83, doi: 10.3847/1538-4357/aa6e52

Douglas, S. T., Curtis, J. L., Agüeros, M. A., et al. 2019, ApJ, 879, 100, doi: 10.3847/1538-4357/ab2468

El-Badry, K., Rix, H.-W., & Heintz, T. M. 2021, MNRAS, 506, 2269, doi: 10.1093/mnras/stab323

Feiden, G. A., & Chaboyer, B. 2012, ApJ, 761, 30, doi: 10.1088/0004-637X/761/1/30

Ford, E. B., Ragozzine, D., Rowe, J. F., et al. 2012, ApJ, 756, 185, doi: 10.1088/0004-637X/756/2/185

Foreman-Mackey, D. 2016, The Journal of Open Source Software, 1

Foreman-Mackey, D., Agol, E., Ambikasaran, S., & Angus, R. 2017, AJ, 154, 220, doi: 10.3847/1538-3881/aa9332

Foreman-Mackey, D., Hogg, D. W., Lang, D., & Goodman, J. 2013, PASP, 125, 306, doi: 10.1086/670067

Gagné, J., Faherty, J. K., Moranta, L., & Popinchalk, M. 2021, ApJL, 915, L29, doi: 10.3847/2041-8213/ac0e9a

Gagné, J., Mamajek, E. E., Malo, L., et al. 2018, ApJ, 856, 23, doi: 10.3847/1538-4357/aaae09

Gaia Collaboration, Prusti, T., de Bruijne, J. H. J., et al. 2016, A&A, 595, A1, doi: 10.1051/0004-6361/201629272

Gaia Collaboration, Brown, A. G. A., Vallenari, A., et al. 2021, A&A, 649, A1, doi: 10.1051/0004-6361/202039657

Gaidos, E., Mann, A. W., Rizzuto, A., et al. 2017, MNRAS, 464, 850, doi: 10.1093/mnras/stw2345

Giles, H. A. C., Collier Cameron, A., & Haywood, R. D. 2017, MNRAS, 472, 1618, doi: 10.1093/mnras/stx1931

Gray, D. F. 1992, The observation and analysis of stellar photospheres., Vol. 10 (Camb. Astrophys. Ser)

Green, G. M., Schlafly, E., Zucker, C., Speagle, J. S., & Finkbeiner, D. 2019, ApJ, 887, 93, doi: 10.3847/1538-4357/ab5362

Hattori, S., Foreman-Mackey, D., Hogg, D. W., et al. 2021, arXiv e-prints, arXiv:2106.15063. https://arxiv.org/abs/2106.15063

Henden, A. A., Templeton, M., Terrell, D., et al. 2016, VizieR Online Data Catalog, II/336

Hogg, D. W., Bovy, J., & Lang, D. 2010, arXiv e-prints, arXiv:1008.4686. https://arxiv.org/abs/1008.4686

Holczer, T., Mazeh, T., Nachmani, G., et al. 2016, ApJS, 225, 9, doi: 10.3847/0067-0049/225/1/9

Horne, J. H., & Baliunas, S. L. 1986, ApJ, 302, 757, doi: 10.1086/164037

Huang, C. X., Vanderburg, A., Pál, A., et al. 2020, Research Notes of the American Astronomical Society, 4, 204, doi: 10.3847/2515-5172/abca2e

Hunter, J. D. 2007, Computing in science & engineering, 9, 90

Husser, T.-O., Wende-von Berg, S., Dreizler, S., et al. 2013, A&A, 553, A6, doi: 10.1051/0004-6361/201219058

Jenkins, J. M., Caldwell, D. A., Chandrasekaran, H., et al. 2010, ApJL, 713, L120, doi: 10.1088/2041-8205/713/2/L120

Johnson, J. A., Petigura, E. A., Fulton, B. J., et al. 2017, AJ, 154, 108, doi: 10.3847/1538-3881/aa80e7

Johnson, M. C., Dai, F., Justesen, A. B., et al. 2018, MNRAS, 481, 596, doi: 10.1093/mnras/sty2238

Jönsson, H., Holtzman, J. A., Allende Prieto, C., et al. 2020, AJ, 160, 120, doi: 10.3847/1538-3881/aba592

Katz, D., Sartoretti, P., Cropper, M., et al. 2019, A&A, 622, A205, doi: 10.1051/0004-6361/201833273

Kerr, R., Rizzuto, A. C., Kraus, A. L., & Offner, S. S. R. 2021, arXiv e-prints, arXiv:2105.09338. https://arxiv.org/abs/2105.09338

Kiman, R., Faherty, J. K., Cruz, K. L., et al. 2021, arXiv e-prints, arXiv:2104.01232. https://arxiv.org/abs/2104.01232

Kipping, D. M. 2013, MNRAS, 435, 2152, doi: 10.1093/mnras/stt1435

Kounkel, M., & Covey, K. 2019, AJ, 158, 122, doi: 10.3847/1538-3881/ab339a

Kounkel, M., Covey, K., & Stassun, K. G. 2020, AJ, 160, 279, doi: 10.3847/1538-3881/abc0e6

Kraus, A. L., Ireland, M. J., Huber, D., Mann, A. W., & Dupuy, T. J. 2016, AJ, 152, 8, doi: 10.3847/0004-6256/152/1/8

Kreidberg, L. 2015, PASP, 127, 1161, doi: 10.1086/683602

Krumholz, M. R., McKee, C. F., & Bland-Hawthorn, J. 2019, ARA&A, 57, 227, doi: 10.1146/annurev-astro-091918-104430

Li, C., Zhao, G., Zhai, M., & Jia, Y. 2018, ApJ, 860, 53, doi: 10.3847/1538-4357/aac50f

Lim, P. L. 2020, synphot, 1.0.1, Zenodo, doi: 10.5281/zenodo.3971036

Luo, A. L., Zhao, Y. H., Zhao, G., & et al. 2019, VizieR Online Data Catalog, V/164

Luo, A. L., Zhao, Y.-H., Zhao, G., et al. 2015, Research in Astronomy and Astrophysics, 15, 1095, doi: 10.1088/1674-4527/15/8/002

Mann, A. W., Gaidos, E., Mace, G. N., et al. 2016a, ApJ, 818, 46, doi: 10.3847/0004-637X/818/1/46

Mann, A. W., Newton, E. R., Rizzuto, A. C., et al. 2016b, AJ, 152, 61, doi: 10.3847/0004-6256/152/3/61

Mann, A. W., Dupuy, T., Muirhead, P. S., et al. 2017a, AJ, 153, 267, doi: 10.3847/1538-3881/aa7140

Mann, A. W., Gaidos, E., Vanderburg, A., et al. 2017b, AJ, 153, 64, doi: 10.1088/1361-6528/aa5276

Mann, A. W., Dupuy, T., Kraus, A. L., et al. 2019, ApJ, 871, 63, doi: 10.3847/1538-4357/aaf3bc

Mann, A. W., Wood, M. L., Schmidt, S. P., et al. 2021, arXiv e-prints, arXiv:2110.09531. https://arxiv.org/abs/2110.09531

Masuda, K., & Winn, J. N. 2020, AJ, 159, 81, doi: 10.3847/1538-3881/ab65be

McQuillan, A., Aigrain, S., & Mazeh, T. 2013, MNRAS, 432, 1203, doi: 10.1093/mnras/stt536

McQuillan, A., Mazeh, T., & Aigrain, S. 2014, ApJS, 211, 24, doi: 10.1088/0067-0049/211/2/24

Meibom, S., Barnes, S. A., Latham, D. W., et al. 2011, ApJL, 733, L9, doi: 10.1088/2041-8205/733/1/L9

Meibom, S., Torres, G., Fressin, F., et al. 2013, Nature, 499, 55, doi: 10.1038/nature12279

Meingast, S., Alves, J., & Fürnkranz, V. 2019, A&A, 622, L13, doi: 10.1051/0004-6361/201834950

Miglio, A., Brogaard, K., Stello, D., et al. 2012, MNRAS, 419, 2077, doi: 10.1111/j.1365-2966.2011.19859.x

Morton, T. D. 2015a, isochrones: Stellar model grid package. http://ascl.net/1503.010

—. 2015b, VESPA: False positive probabilities calculator, Astrophysics Source Code Library. http://ascl.net/1503.011

Morton, T. D., Bryson, S. T., Coughlin, J. L., et al. 2016, ApJ, 822, 86, doi: 10.3847/0004-637X/822/2/86

Morton, T. D., & Winn, J. N. 2014, ApJ, 796, 47, doi: 10.1088/0004-637X/796/1/47

NASA Exoplanet Science Institute. 2020, Planetary Systems Table, IPAC, doi: 10.26133/NEA12

Newton, E. R., Mann, A. W., Tofflemire, B. M., et al. 2019, ApJL, 880, L17, doi: 10.3847/2041-8213/ab2988

Newton, E. R., Mann, A. W., Kraus, A. L., et al. 2021, AJ, 161, 65, doi: 10.3847/1538-3881/abccc6

Nielsen, M. B., Gizon, L., Schunker, H., & Karoff, C. 2013, A&A, 557, L10, doi: 10.1051/0004-6361/201321912

Owen, J. E. 2020, MNRAS, 498, 5030, doi: 10.1093/mnras/staa2784

Parviainen, H., & Aigrain, S. 2015, MNRAS, 453, 3821, doi: 10.1093/mnras/stv1857

Pecaut, M. J., & Mamajek, E. E. 2013, ApJS, 208, 9, doi: 10.1088/0067-0049/208/1/9

Petigura, E. A. in prep, AJ

Petigura, E. A., Howard, A. W., Marcy, G. W., et al. 2017, AJ, 154, 107, doi: 10.3847/1538-3881/aa80de

Rampalli, R., Agüeros, M. A., Curtis, J. L., et al. 2021, arXiv e-prints, arXiv:2106.13250. https://arxiv.org/abs/2106.13250

Rebull, L. M., Stauffer, J. R., Bouvier, J., et al. 2016a, AJ, 152, 113, doi: 10.3847/0004-6256/152/5/113

—. 2016b, AJ, 152, 114, doi: 10.3847/0004-6256/152/5/114

Riello, M., De Angeli, F., Evans, D. W., et al. 2021, A&A, 649, A3, doi: 10.1051/0004-6361/202039587

Rizzuto, A. C., Mann, A. W., Vanderburg, A., Kraus, A. L., & Covey, K. R. 2017, AJ, 154, 224, doi: 10.3847/1538-3881/aa9070

Santos, A. R. G., Breton, S. N., Mathur, S., & García, R. A. 2021, ApJS, 255, 17, doi: 10.3847/1538-4365/ac033f

Santos, A. R. G., García, R. A., Mathur, S., et al. 2019, ApJS, 244, 21, doi: 10.3847/1538-4365/ab3b56

Schlafly, E. F., & Finkbeiner, D. P. 2011, ApJ, 737, 103, doi: 10.1088/0004-637X/737/2/103

Skrutskie, M. F., Cutri, R. M., Stiening, R., et al. 2006, AJ, 131, 1163, doi: 10.1086/498708

Smith, J. C., Stumpe, M. C., Van Cleve, J. E., et al. 2012, PASP, 124, 1000, doi: 10.1086/667697

Stanford-Moore, S. A., Nielsen, E. L., De Rosa, R. J., Macintosh, B., & Czekala, I. 2020, ApJ, 898, 27, doi: 10.3847/1538-4357/ab9a35

Stassun, K. G., Oelkers, R. J., Pepper, J., et al. 2018, AJ, 156, 102, doi: 10.3847/1538-3881/aad050

Stassun, K. G., Oelkers, R. J., Paegert, M., et al. 2019, AJ, 158, 138, doi: 10.3847/1538-3881/ab3467

Stumpe, M. C., Smith, J. C., Van Cleve, J. E., et al. 2012, PASP, 124, 985, doi: 10.1086/667698

Tofflemire, B. M., Mathieu, R. D., & Johns-Krull, C. M. 2019, AJ, 158, 245, doi: 10.3847/1538-3881/ab4f7d

Tofflemire, B. M., Rizzuto, A. C., Newton, E. R., et al. 2021, AJ, 161, 171, doi: 10.3847/1538-3881/abdf53

Tran, Q. H., Bowler, B. P., Cochran, W. D., et al. 2021, AJ, 161, 173, doi: 10.3847/1538-3881/abe041

Tull, R. G., MacQueen, P. J., Sneden, C., & Lambert, D. L. 1995, PASP, 107, 251, doi: 10.1086/133548

Twicken, J. D., Jenkins, J. M., Seader, S. E., et al. 2016, AJ, 152, 158, doi: 10.3847/0004-6256/152/6/158

Van Cleve, J. E., Howell, S. B., Smith, J. C., et al. 2016, PASP, 128, 075002, doi: 10.1088/1538-3873/128/965/075002

van Saders, J. L., Ceillier, T., Metcalfe, T. S., et al. 2016, Nature, 529, 181, doi: 10.1038/nature16168

Walkowicz, L. M., & Basri, G. S. 2013, MNRAS, 436, 1883, doi: 10.1093/mnras/stt1700

Wood, M. L., Mann, A. W., & Kraus, A. L. 2021, AJ, 162, 128, doi: 10.3847/1538-3881/ac0ae9

Yee, S. W., Petigura, E. A., & von Braun, K. 2017, ApJ, 836, 77, doi: 10.3847/1538-4357/836/1/77

Ziegler, C., Tokovinin, A., Briceño, C., et al. 2020, AJ, 159, 19, doi: 10.3847/1538-3881/ab55e9

**Table 5.**

| Gaia EDR3 | α (J2016) | δ (J2016) | Gmag (mag) | $V_{off}$ (km/s) | Spectral[a] Class | TESS[b] | Kepler[b] | π (mas) | $\sigma_\pi$ (mas) | $P_{rot}$ (days) | $\sigma_{P_{rot}}$ (days) | $P_{rot}$[c] ref | Li (mÅ) | $\sigma_{li}$ (mÅ) | RV (km/s) | $\sigma_{RV}$ (km/s) | RV[d] ref |
|---|---|---|---|---|---|---|---|---|---|---|---|---|---|---|---|---|---|
| 2052827207364859264 | 290.44063 | 38.52357 | 12.605 | 0.000 | G7.3 | Y | Y | 3.057 | 0.009 | 4.665 | 0.035 | 2, 3 | 134.0 | 18.0 | -26.09 | 0.03 | 5 |
| 2101379205604338688 | 289.62522 | 40.70874 | 14.788 | 3.102 | K5.3 | N | Y | 3.015 | 0.019 | 9.23 | 0.66 | 3 | <40 | ... | -27.15 | 0.1 | 9 |
| 2052804323776522624 | 290.46921 | 38.20201 | 18.977 | 3.554 | M3.9 | N | N | 3.036 | 0.172 | ... | ... | ... | ... | ... | ... | ... | ... |
| 2100939194794324608 | 289.80783 | 38.95042 | 10.829 | 0.478 | F4.4 | Y | N | 3.024 | 0.012 | ... | ... | ... | ... | ... | -27.03 | 0.18 | 5 |
| 2052954995531623040 | 291.28017 | 39.20070 | 14.355 | 4.348 | K4.7 | N | Y | 3.055 | 0.016 | 13.849 | 0.035 | 1, 2, 3 | <20 | ... | ... | ... | ... |
| 2100967537279486336 | 290.14895 | 39.26079 | 18.451 | 3.806 | M4.1 | N | N | 3.094 | 0.136 | ... | ... | ... | ... | ... | ... | ... | ... |
| 2051102868195719168 | 290.43983 | 37.73210 | 17.503 | 0.516 | M3.2 | N | N | 3.019 | 0.069 | ... | ... | ... | ... | ... | ... | ... | ... |
| 2053037660761796096 | 290.86832 | 39.65124 | 17.902 | 0.605 | M3.7 | N | N | 3.067 | 0.084 | ... | ... | ... | ... | ... | ... | ... | ... |
| 2052645379929910144 | 290.91118 | 38.33558 | 13.747 | 0.988 | K2.8 | N | Y | 2.996 | 0.033 | 7.84 | 0.784 | 4 | ... | ... | -27.05 | 3.02 | 6 |
| 2052559959597846208 | 291.61221 | 37.79730 | 11.75 | 3.744 | F9.3 | Y | Y | 3.082 | 0.01 | 10.55 | 0.552 | 1, 3 | ... | ... | -16.07 | 0.95 | 7 |
| 2100996639982248320 | 289.86923 | 39.64549 | 19.678 | 2.692 | M3.7 | N | N | 3.083 | 0.322 | ... | ... | ... | ... | ... | ... | ... | ... |
| 2099426507311747200 | 289.44803 | 38.58778 | 17.385 | 0.897 | M3.1 | N | N | 3.114 | 0.07 | ... | ... | ... | ... | ... | ... | ... | ... |
| 2052684790548985728 | 291.78531 | 38.46727 | 14.077 | 0.641 | K4.6 | N | N | 3.009 | 0.038 | ... | ... | ... | ... | ... | ... | ... | ... |
| 2052853072267403520 | 290.54042 | 38.81248 | 11.42 | 0.350 | F9.4 | N | Y | 2.978 | 0.019 | 4.419 | 0.347 | 2 | <70 | ... | -25.11 | 0.16 | 5 |
| 2053046907832580992 | 291.12056 | 39.64699 | 16.939 | 0.389 | M2.6 | N | N | 3.003 | 0.046 | ... | ... | ... | ... | ... | ... | ... | ... |
| 2099289446315734784 | 288.78892 | 37.90815 | 10.835 | 0.240 | F4.3 | Y | N | 3.099 | 0.011 | ... | ... | ... | <20 | ... | -27.46 | 0.13 | 5 |
| 2053001690416510720 | 291.56724 | 39.60279 | 18.441 | 0.159 | M4.5 | N | N | 3.104 | 0.122 | ... | ... | ... | ... | ... | ... | ... | ... |
| 2052887478644057472 | 289.93506 | 38.64045 | 14.636 | 0.506 | K5.3 | N | Y | 3.145 | 0.018 | 1.529 | 0.017 | 1, 2, 3 | ... | ... | -30.74 | 5.17 | 6 |
| 2052807794117101312 | 290.53790 | 38.25958 | 14.736 | 3.776 | K5.4 | Y | Y | 2.971 | 0.031 | 7.595 | 0.222 | 1, 2, 3 | ... | ... | ... | ... | ... |
| 2052517145084325888 | 291.05028 | 37.29823 | 19.789 | 0.587 | M4.1 | N | N | 3.002 | 0.33 | ... | ... | ... | ... | ... | ... | ... | ... |
| 2053028319213859072 | 290.64738 | 39.41039 | 20.044 | 2.510 | M2.4 | N | N | 3.141 | 0.449 | ... | ... | ... | ... | ... | ... | ... | ... |
| 2053384286102387200 | 291.63783 | 39.87497 | 16.359 | 1.316 | M2.7 | N | N | 3.008 | 0.037 | ... | ... | ... | ... | ... | ... | ... | ... |
| 2099371153774293888 | 288.14566 | 38.42085 | 13.864 | 0.791 | K3.3 | N | Y | 3.018 | 0.025 | 7.556 | 0.049 | 1, 2, 3 | ... | ... | -33.36 | 10.0 | 6 |
| 2053444896681432704 | 291.46297 | 40.21305 | 17.606 | 4.287 | M3.8 | N | N | 3.093 | 0.076 | ... | ... | ... | ... | ... | ... | ... | ... |
| 2051172511083958400 | 289.48378 | 37.33728 | 20.024 | 1.298 | M2.3 | N | N | 3.137 | 0.394 | ... | ... | ... | ... | ... | ... | ... | ... |

NOTE—Table 5 is truncated. The full version will be available online.

[a] Spectral types are assigned based on the star's $B_P - R_P$ color and the table from Pecaut & Mamajek (2013).

[b] Indicates if the target had a light curve in TESS or Kepler of sufficient quality for running the Notch transit-search pipeline.

[c] Key for rotation period references: 1 = (McQuillan et al. 2013, 2014), 2 = (Nielsen et al. 2013), 3 = Santos et al. (2021, 2019), 4 = This work

[d] Key for radial velocity references: 5 = Coude, 6 = LAMOSTDR5 (Luo et al. 2019), 7 = Gaia DR2 (Katz et al. 2019), 8 = APOGEE DR16 (Jönsson et al. 2020), 9 = CKS (Petigura in prep)